Hindawi
International Journal of Aerospace Engineering
Volume 2024, Article ID 2249954, 28 pages
https://doi.org/10.1155/2024/2249954

Research Article

Numerical Study on the Self-Pulsation Characteristics of LOX/GH_2 Swirl Coaxial Injector

Wentong Qiao,[1] **Chengkai Liang**,[1] **Luhao Liu**,[1] **Shaoyan Wang**,[1] **Bingbing Zhang**,[1] **Xiaocong Yang**,[1] **Lijun Yang**,[1] **and Qingfei Fu**[1,2]

[1]*School of Astronautics, Beihang University, Beijing 100191, China*
[2]*Ningbo Institute of Technology, Beihang University, Ningbo 315100, China*

Correspondence should be addressed to Qingfei Fu; fuqingfei@buaa.edu.cn

Received 13 July 2023; Revised 29 January 2024; Accepted 20 February 2024; Published 15 March 2024

Academic Editor: Zhiguang Song

To investigate the self-pulsation characteristics of a liquid-centered swirl coaxial injector with liquid oxygen (LOX) and gas hydrogen (GH_2) as the working mediums under supercritical condition, a numerical simulation was employed. The transient simulation of the flow and injection process of cryogenic propellant was carried out using the RNG $k-\varepsilon$ turbulence model, VOF model, and Peng-Robinson equation of state. The frequency spectrum of calculated pressure oscillation agreed with the experimental data. The amplitude-frequency characteristics of recess region, LOX, and GH_2 paths when self-pulsation occurs were analyzed. The effects of operating parameters, such as the flow rate of LOX or GH_2 and the initial GH_2 temperature, on the self-pulsation, were evaluated specifically. Results reveal that the self-pulsation results from the periodic variation of pressure and velocity caused by the periodic blocking of annular gas by the liquid sheet. The dominant frequencies of pressure oscillation in the recess region, upstream of LOX, or GH_2 path are diverse. But for the points in each region, the dominant frequency is about the same. When the LOX/GH_2 mixing ratio increases, the liquid sheet thickness and the number of liquid filaments increase. The position where filaments are massively broken into droplets moves further downstream. For the same mixing ratio, the flow rate of LOX has a greater impact on the atomization features. The pressures corresponding to low or high frequency increase when the initial GH_2 temperature raises. The higher temperature would shift the dominant oscillation between the low and high regimes.

1. Introduction

The atomization performance of the liquid-centered swirl coaxial (LCSC) injector is superior due to the shearing effect between the gas and the centrifugal liquid sheet, so it is widely used in liquid rocket engines, such as YF-73, YF-75, RL10-A, and RD-57 [1–3]. However, due to the collision between the gas and liquid sheet being too violent in the recess chamber of the injector, it may cause the pressure and flow rate constantly varying at the injector outlet. This is reflected in the periodic oscillation of the liquid phase in the spray field, which is called self-pulsation phenomenon [4–6]. Self-pulsation oscillation could greatly affect the propellant atomization process and would cause a strong whistling sound at the injector outlet. The pressure and flow oscillations caused by self-pulsation oscillations in the injector may be coupled with acoustic oscillations generated by the injector or other structures, such as the injection panel or combustion chamber. Once this coupling occurs, unstable combustion may be initiated, which in turn damages the structure of the combustion chamber. It may even increase the rate of combustion, which can lead to destruction of the combustion chamber walls and damage the entire thrust system [7, 8]. Therefore, attenuating combustion instability by means of suppressing the self-pulsation oscillations of the injector is essential for improving engine safety.

The characteristics and the mechanism of self-pulsation have been the focus of many scholars' research for a long time. Self-pulsation phenomenon is mainly manifested as a constant oscillation in pressure and flow rate at some locations of the injector resulting from the time-delayed feedback of the gas and liquid collision [5, 9]. Based on this, Bazarov [6] proposed a linear theoretical model that views

the liquid sheet as a flexible valve flap. The gas flow can change its position and shape. The gap between the liquid sheet and the inner wall of the injector fluctuates with the variation of the gas flow velocity, thus generating pressure fluctuations in the inlet channel. Eberhart et al. [10, 11] further analyzed that the swirl injector has a hydraulic instability, and this hydraulic instability and self-excited oscillations are highly related. When the injector is sensitive to changes in some fluid parameters near the outlet, it is likely to produce self-pulsation oscillations due to the hydraulic instability. However, Bai et al. [4] suggested that the self-pulsation is caused by the periodic blocking effect of the conical liquid sheet, resulting in periodic pressure oscillation inside the recess chamber. The pressure reacts to the liquid sheet and then causes it to oscillate. The self-pulsation is described as liquid film periodically blocking gas-type self-pulsation and gas periodically squeezing liquid film-type self-pulsation according to the oscillation frequency of self-pulsation before and after the abrupt crossing. Furthermore, Huang et al. [12] proposed that the mechanism of self-pulsation is that the vortex shedding at the inlet of the hydrogen injector induces an acoustic resonance between the annular slit gas and the gas vortex at the center of the liquid injector. Based on this, an acoustic model of injector whistling is proposed. The gas flow velocity, the sound velocity of the gas hollow, and the ratio of the length of gas annulus to that of gas hollow will affect the resonance.

For the LCSC injector with liquid oxygen (LOX) and gaseous hydrogen (GH_2) as the working medium, the self-pulsation phenomenon would occur under specific geometric structure and operating conditions. In recent years, many simulations [13–16] and experimental [17–19] studies have been conducted to explore the effect on the amplitude and frequency characteristics of self-pulsation oscillations by varying some structural parameters of the injector, or by changing the operating conditions. Investigations on the structure parameters have focused on the width of the gas annular slit [17], the length of the recess section of the inner injector [19, 20], the diameter of the inner injector [5], and the size of the gas nucleus formed during injector operation [20, 21], all of which can change the amplitude and frequency characteristics of self-pulsation. Im et al. [5] found that the self-pulsation is suppressed when the gas annular slit width increases, while the gas flow is blocked by the liquid sheet when the annular slit width decreases. The gas-liquid phase interaction is enhanced, and the intensity of self-excited oscillations is increased. By numerical simulation and some experiments at ambient temperature for LCSC injector, Bai et al. [4] found that if the annular slit width becomes larger when the gas-liquid ratio is very small, then the self-pulsation will become weaker. If the annular slit width becomes larger again when the gas-liquid ratio is not that small, the self-pulsation will not become weaker as described earlier. In terms of the recess length of the inner injector, Bazarov [6] found through experimental studies that when the recess length is not zero, the injector will generate self-pulsation. However, if the recess length is zero, that is, there is no recess section, then the injector in operation will be in a stable state, and no self-pulsation will occur. Eberhart [22] found that both recess and nonrecess injector will occur self-pulsation oscillation. Self-pulsation is more pronounced with recess, which means that the recess of internal injector is not a necessary condition to generate self-pulsation. In terms of gas nucleus size, Im and Yoon [21] studied that at small gas nucleus sizes, the conical liquid film produced dominant surface waves and violently collided with the annular gas. This interaction would cause the self-pulsation. The liquid sheet excited by self-pulsation breaks section by section, producing many liquid filaments and blocks. These liquid filaments come into contact at the center of the injector and then appear in the shape of a "string" after collision. Kang et al. [20] also studied the effect of this aspect and found that if the size of the gas nucleus is relatively large, the spray will not break to form many liquid filaments as described earlier but will continuously form a ring-like liquid ligament.

To summarize the above, most of the current studies focus on the structure of the injector. However, there are relatively few studies on the effect of operating conditions on the self-pulsation characteristics, which only mainly involve the backpressure, gas-liquid ratio, and real hot test conditions. Im and Yoon [21] pointed out that the backpressure can significantly suppress the dominant surface waves of the liquid sheet, which leads to the suppression of self-pulsation. Among the many influencing factors, liquid momentum is the inertial term and suppresses self-excited oscillations. Gas momentum is the perturbation term, which promotes self-excited oscillations. Bai et al. [18] proposed that with the increase of backpressure, self-pulsation is intensified initially and then suppressed, while self-pulsation frequency fluctuates within a certain range. Backpressure affects self-pulsation by transforming the flow pattern in recess chamber and then strengthening or weakening the blocking actions of the conical liquid sheet. By means of numerical simulation, Chu et al. [14] thought that the atomization process becomes dominated successively by the instability of the liquid film, strong gas-liquid interaction, and spray self-pulsation when increasing the gas-liquid ratio. With a larger gas-liquid ratio, self-pulsation occurs, which is found to determine the flow structures inside the spray cone and to generate, shed, and dissipate vortices periodically. Except for the flow rates of each propellant, scholars [23] have found that the self-pulsation can be motivated by the phase change from liquid to vapor which happens when the preheat temperature of the gas flowing through the burner exceeds the boiling temperature at the operating pressure. However, this mechanism of the self-pulsation due to the propellant phase change caused by the temperature change is unclear. For the LOX/GH_2 propellant in the real hot test condition, Qiao [24] employed simulation to analyze the self-pulsation mechanism under supercritical conditions and specifically analyzes the effects of recess length and gas core size on the self-pulsation oscillation. But the effects of LOX/GH_2 flow rate, mixing ratio, and temperature on the self-pulsation characteristics under supercritical conditions are not addressed.

Most of the studies on the self-pulsation of LCSC injector are focused on the ambient temperature conditions, and the research on the self-pulsation for the cryogenic fluids, such as LOX and GH_2, under supercritical conditions is scarce. There is still a lack of understanding of the self-pulsation mechanism under such supercritical conditions. However, when the propellant used in a rocket engine is sprayed from

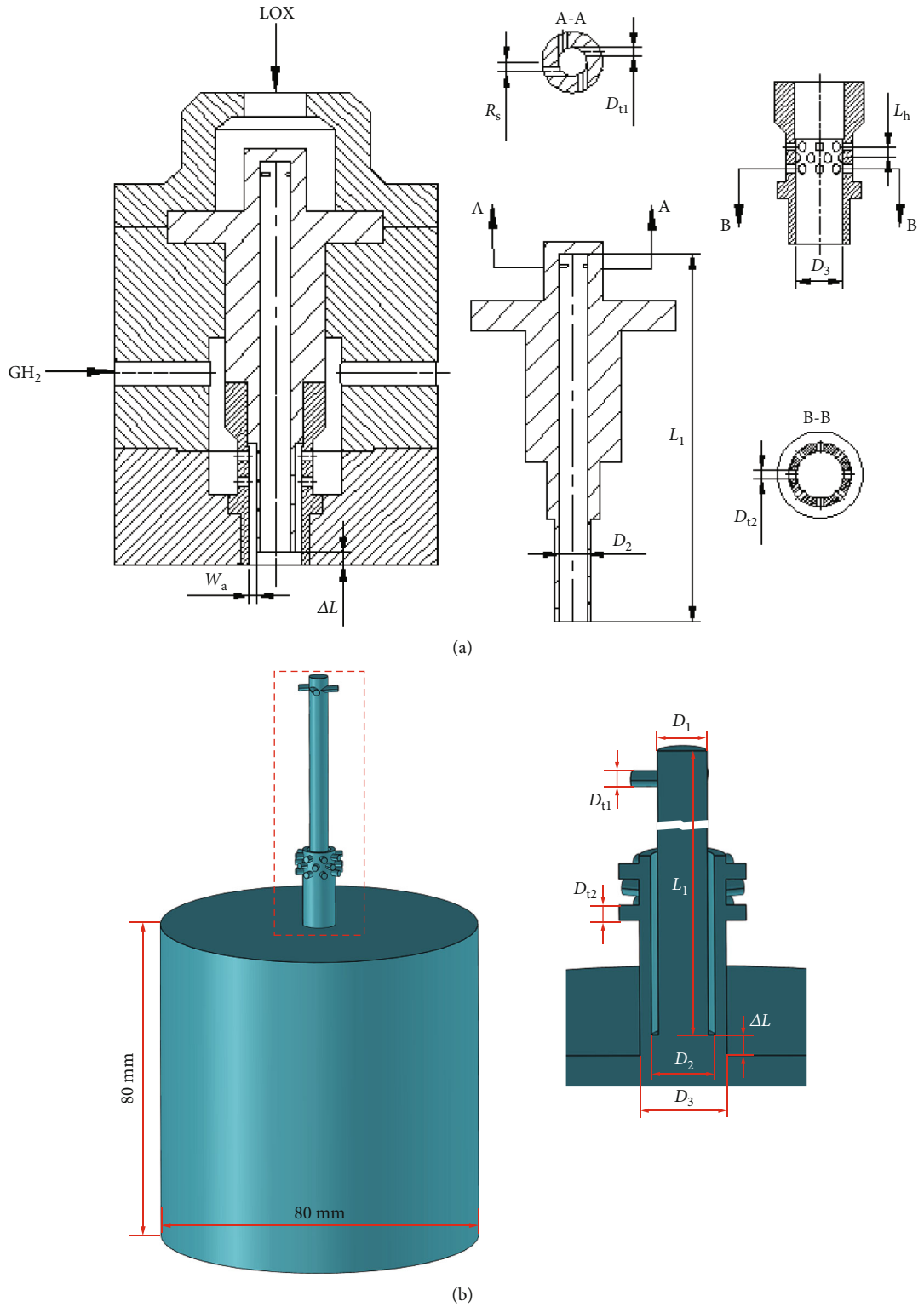

Figure 1: LOX/GH_2 swirl coaxial injector: (a) injector assembly; (b) three-dimensional fluid domain.

the storage tank to the combustion chamber, its flow condition is exactly in a supercritical state. In this paper, with the intents of analyzing the mechanism of self-pulsation for LCSC injector with LOX and GH_2 as the working medium under supercritical conditions and to study the self-pulsation characteristics at various parts (such as recess region, LOX path, and GH_2 path) of the injector, a simulation model is developed. In addition, the effects of the operating conditions such as the flow rates of LOX and GH_2, the LOX/GH_2 mixing ratio, and the initial GH_2 temperature on the self-pulsation characteristics are also analyzed specifically.

Table 1: Geometrical parameters of the LOX/GH_2 swirl coaxial injector.

	Dimensionless parameters	Values
Inner injector	D_1/D_1	1
	L_1/D_1	13.15
	D_{t1}/D_1	0.32
	R_s/D_1	0.34
	D_2/D_1	1.28
Outer injector	D_3/D_1	1.74
	D_{t2}/D_1	0.32
	L_h/D_1	0.43
Recess region	$\Delta L/D_1$	0.43

Note: D_1 is the diameter of swirl chamber, i.e., the reference size; L_1 is the length of swirl chamber; D_{t1} is the diameter of tangential hole, the number of which is 4; R_s is the swirl radius; D_2 is the outer diameter of inner injector; D_3 is the diameter of outer injector outlet; D_{t2} is the diameter of inlet hole, the number of which is 8×3 row; L_h is the distance between each row of inlet holes; ΔL is the recess length.

2. Numerical Setup

2.1. Injector Model. As depicted in Figure 1(a), the liquid oxygen (LOX)/gas hydrogen (GH_2) injector involved in this paper is a liquid-centered swirl coaxial injector, which has the same construction as the injector in reference [24]. The inner part is a liquid pressure-swirl injector, which is fed with a cryogenic fluid, (i.e., liquid oxygen) from four tangential holes. The outer part is a gas direct-current injector, which is fed with gaseous hydrogen from outer multiholes. The liquid is driven by pressure and rotates through the tangential hole of the inner injector into the swirl chamber. The liquid rotates against the wall to form a swirl liquid film, and a gas hollow vortex is formed in the center of the injector channel. After the liquid film flows out of the inner injector, its tangential velocity is gradually converted into radial velocity. The liquid film thickness gradually decreases, and the liquid film expands to form a conical liquid film. The gas is driven by pressure through the outer injector into the annular gap between the outer and inner injectors and collides with the conical liquid film at the recess region. Under the action of centrifugal force and gas-liquid shear, the conical liquid film is destabilized, broken, and atomized. The three-dimensional fluid of the flow channel inside the injector is shown in Figure 1. The dimensionless geometrical parameters of the injector are listed in Table 1, in which the reference size of the diameter of swirl chamber D_1 is 4.7 mm. The typical operating conditions in real hot test are listed in Table 2.

The physical properties of real fluid for LOX and GH_2 propellants are considered in this study. The critical point of oxygen is 154.58 K and 5.043 MPa. The critical point of hydrogen is 33.19 K and 1.313 MPa. According to the operating conditions in Table 2, when the working substance is injected through the injector, the pressure of the working substance (i.e., oxygen) in the inner injector reaches the supercritical state, and the temperature does not reach the supercritical state, which is liquid. The working substance (i.e., hydrogen) in the outer injector reaches the supercritical state for both pressure and temperature, which is a gas-like state.

Table 2: Operating conditions of the LOX/GH2 swirl coaxial injector in hot test.

Operating conditions	Values
Flow rate of $GH_2 \dot{m}_g$ (g/s)	161
Flow rate of LOX $\dot{m}_l$ (g/s)	134
Temperature of GH_2 inlet (K)	33.7
Temperature of LOX inlet (K)	116.2
Ambient pressure (MPa)	8.68
Ambient temperature (K)	800

2.2. Mathematical Model

2.2.1. Turbulence Model. In the spray field of the gas-liquid swirl coaxial injector, there is strong cyclonic flow in the liquid film, and the physical parameters at the gas-liquid interface change rapidly, so the RNG $k-\varepsilon$ model is used for the turbulence model in the numerical simulation [25, 26]. The mathematical method of renormalization group (RNG) used in this model is derived from the transient Navier-Stokes equation. The RNG $k-\varepsilon$ model has good computational power for strong cyclonic flow because the effect of cyclonic flow on turbulence is incorporated in this model. The RNG theory provides analytical formulas for the Prandtl number of the turbulence unlike the standard $k-\varepsilon$ model, which is specified by the user. Further, although the $k-\varepsilon$ model is generally used in the case of a high Reynolds number, the RNG $k-\varepsilon$ model takes into account the effect of a low Reynolds number and is still applicable in the case of the low Reynolds number [27, 28]. Therefore, for the research object of this paper, the RNG $k-\varepsilon$ model is calculated more accurately and reliably compared to the standard $k-\varepsilon$ model. The governing equations for the turbulent kinetic energy k and its dissipation rate ε in RNG $k-\varepsilon$ model are, respectively,

$$\begin{aligned}
\frac{\partial}{\partial t}(\rho k) + \frac{\partial}{\partial x_i}(\rho k u_i) &= \frac{\partial}{\partial x_j}\left(\alpha_k \mu_{\text{eff}} \frac{\partial k}{\partial x_j}\right) + G_k + G_b - \rho\varepsilon - Y_M + S_k, \\
\frac{\partial}{\partial t}(\rho \varepsilon) + \frac{\partial}{\partial x_i}(\rho \varepsilon u_i) &= \frac{\partial}{\partial x_j}\left(\alpha_\varepsilon \mu_{\text{eff}} \frac{\partial \varepsilon}{\partial x_j}\right) + C_{1\varepsilon}\frac{\varepsilon}{k}(G_k + C_{3\varepsilon} G_b) \\
&\quad - C_{2\varepsilon}\rho\frac{\varepsilon^2}{k} - R_\varepsilon + S_\varepsilon,
\end{aligned} \tag{1}$$

where ρ is the fluid density; u_i is the component of the fluid velocity; μ is the viscosity of fluid; G_k is the generation of turbulence kinetic energy due to the mean velocity gradients; G_b is the generation of turbulence kinetic energy due to buoyancy; Y_M is the contribution of the fluctuating dilatation in compressible turbulence to the overall dissipation rate. The quantities α_k and α_ε are the inverse effective Prandtl numbers for k

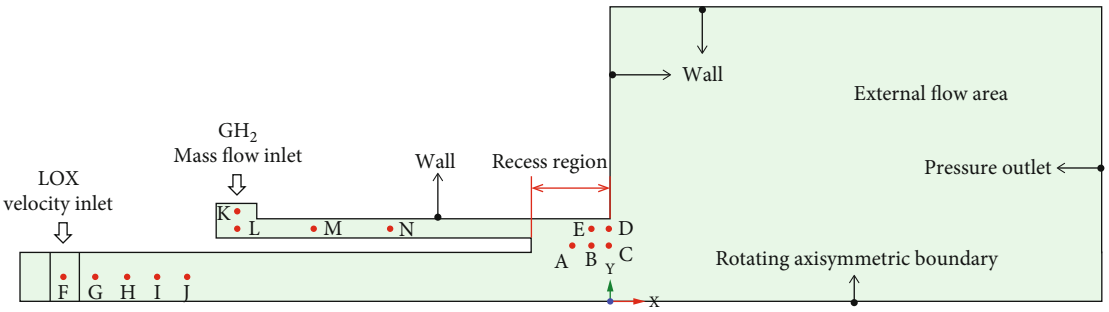

Figure 2: Computing domain and boundary conditions.

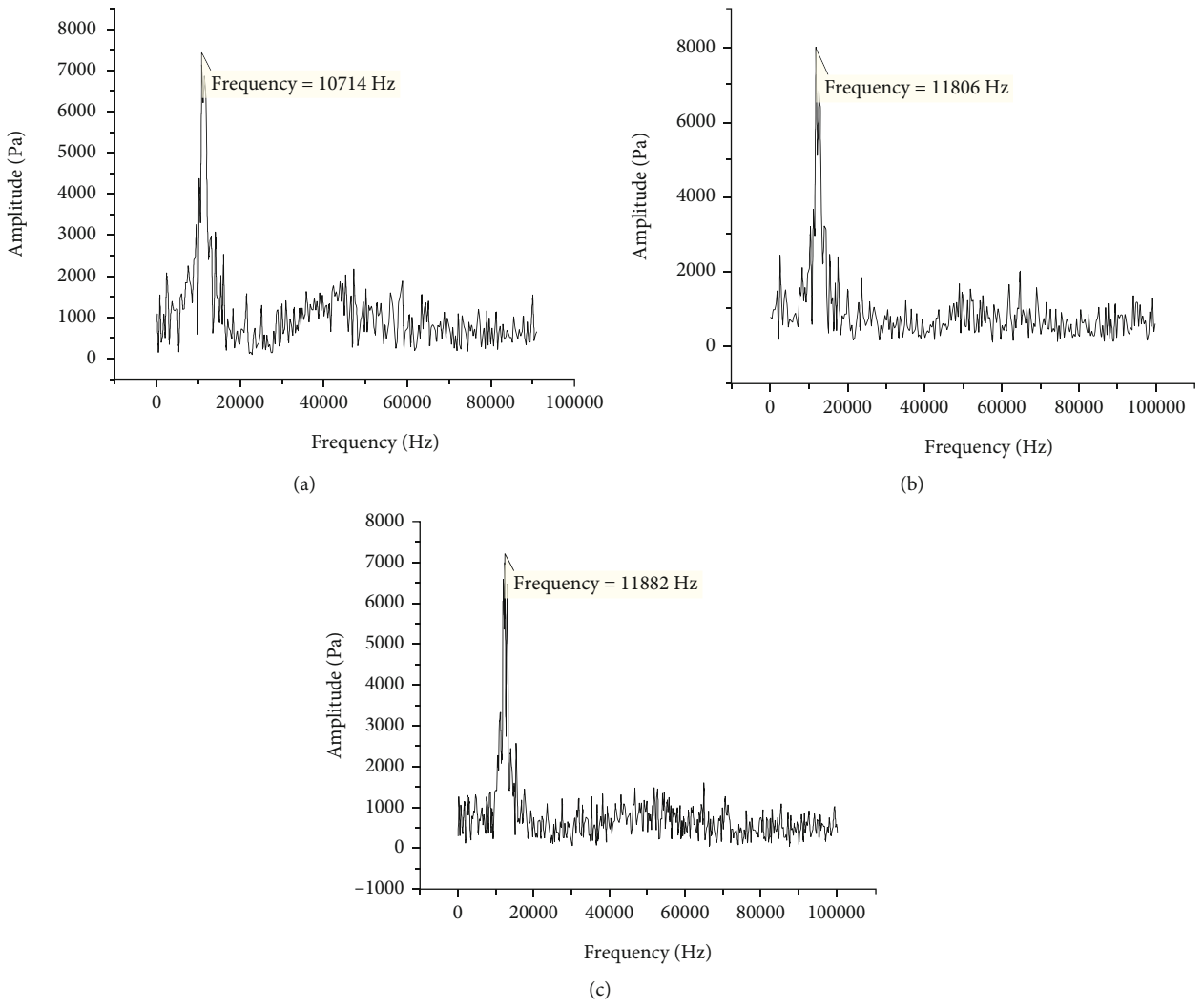

Figure 3: Frequency spectrums of pressure oscillation in the recess region with three different grid systems: (a) coarse grid; (b) intermediate grid; (c) fine grid.

and ε, respectively. At high Reynolds number conditions, $\alpha_k = \alpha_\varepsilon = 1.393$; $C_{1\varepsilon}$ and $C_{2\varepsilon}$ are empirical constants, taken as 1.42 and 1.68, respectively; $C_{3\varepsilon}$ is a constant; S_k and S_ε are other defined source terms; μ_{eff} is the effective viscosity coefficient. R_ε is the additional term added to the governing equation of ε. x_i and x_j are the coordinate components.

2.2.2. VOF Model. The volume of fluid (VOF), as an interface tracking method, assumes that two or more kinds of fluids are not interpenetrating. This model can capture the phase interface between gas and liquid in the injector and easily ensure mass conservation [29]. The VOF model defines the volume fraction α to distinguish the gas and

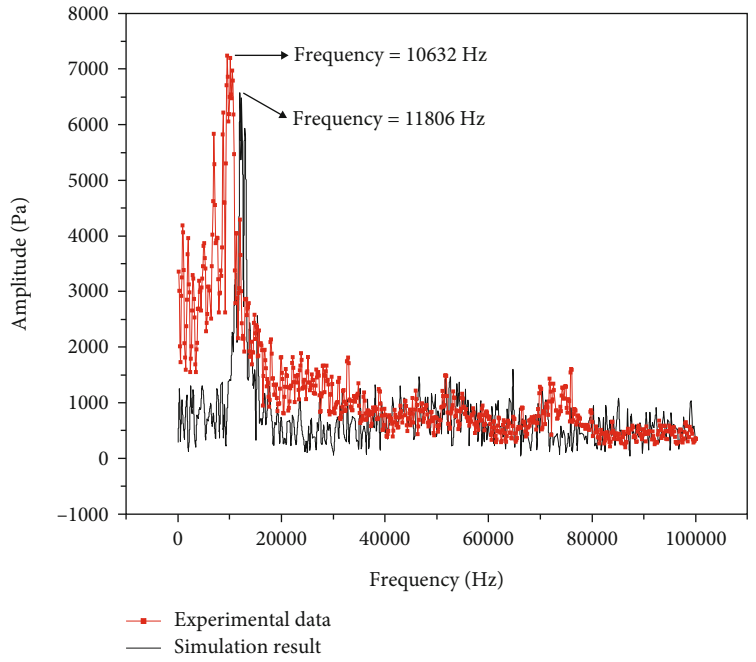

Figure 4: Comparison of simulation result and experimental data.

liquid. The gas is generally defined as the first phase and the liquid as the second phase. When $\alpha = 0$, it is considered that there is no liquid in the whole computational fluid domain. When $\alpha = 1$, there is no gas in the fluid domain. When $0 < \alpha < 1$, it is considered that there is a gas-liquid mixture in the fluid domain [30]. Phase interface tracking is achieved by solving the volume fraction continuity equation, and the transport equation of volume fraction is

$$\begin{aligned} \frac{\partial}{\partial t}\left(\alpha_g \rho_g\right) + \nabla \cdot \left(\alpha_g \rho_g \vec{v}_g\right) &= \left(\dot{m}_{\mathrm{lg}} - \dot{m}_{gl}\right), \\ \frac{\partial}{\partial t}\left(\alpha_l \rho_l\right) + \nabla \cdot \left(\alpha_l \rho_l \vec{v}_l\right) &= \left(\dot{m}_{gl} - \dot{m}_{\mathrm{lg}}\right), \end{aligned} \tag{2}$$

where ρ_g and $\rho_l$are the density of the gas and liquid phase, respectively. α_g and α_l are the volume fraction of the gas and liquid phase, respectively, and $\alpha_l + \alpha_g = 1$. $\vec{v}_g$ and $\vec{v}_l$ are the velocity of the gas and liquid phase, respectively. $\dot{m}_{\mathrm{lg}}$ is the mass flow rate that the liquid converts to the gas. $\dot{m}_{gl}$ is the mass flow rate that the gas converts to the liquid.

The VOF model solves the momentum equation in the entire fluid domain, where the results obtained from the calculation are used by other terms. This greatly improves the efficiency of the calculation. The specific momentum equation is as follows:

$$\frac{\partial}{\partial t}\left(\rho \vec{v}\right) + \nabla \cdot \left(\rho \vec{v} \vec{v}\right) = -\nabla P + \nabla \cdot \left[\mu\left(\nabla \vec{v} + \nabla \vec{v}^{\mathrm{T}}\right)\right] + \rho \vec{g} + \vec{F}, \tag{3}$$

where P and F represent the pressure and surface tension, respectively. The physical parameters in the transport equation are determined by the constituent phases present in the control body, such as the density $\rho = \alpha_g \rho_g + \alpha_l \rho_l$. The other physical parameters are similar. Moreover, the two phases share an energy equation:

$$\frac{\partial}{\partial t}(\rho E) + \nabla \cdot \left[\vec{v}(\rho E + P)\right] = \nabla \cdot (k_{\mathrm{eff}} \nabla T), \tag{4}$$

where k_{eff} is the effective thermal conductivity. E is the energy, and T is the temperature, both of which are mass-averaged variables.

2.2.3. PR State Equations of Gas. When the injector is operated under real test conditions, the temperature and pressure of hydrogen are in a supercritical state. At this point, the ideal gas model is no longer applicable, as the effects of the actual gas must be considered. Most models use a general form of the cubic equation of state to describe the fugacity coefficient:

$$P = \frac{\mathrm{RT}}{V - b} - \frac{a(V - \eta)}{(V - b)\left(V^2 + \delta V + \varepsilon\right)}, \tag{5}$$

where V is the molar volume. In the Peng-Robinson (PR) equation of state, $\delta = 2b$, $\varepsilon = b^2$, and $\eta = b$:

$$P = \frac{\mathrm{RT}}{V - b} - \frac{a}{V^2 + 2bV - b^2}. \tag{6}$$

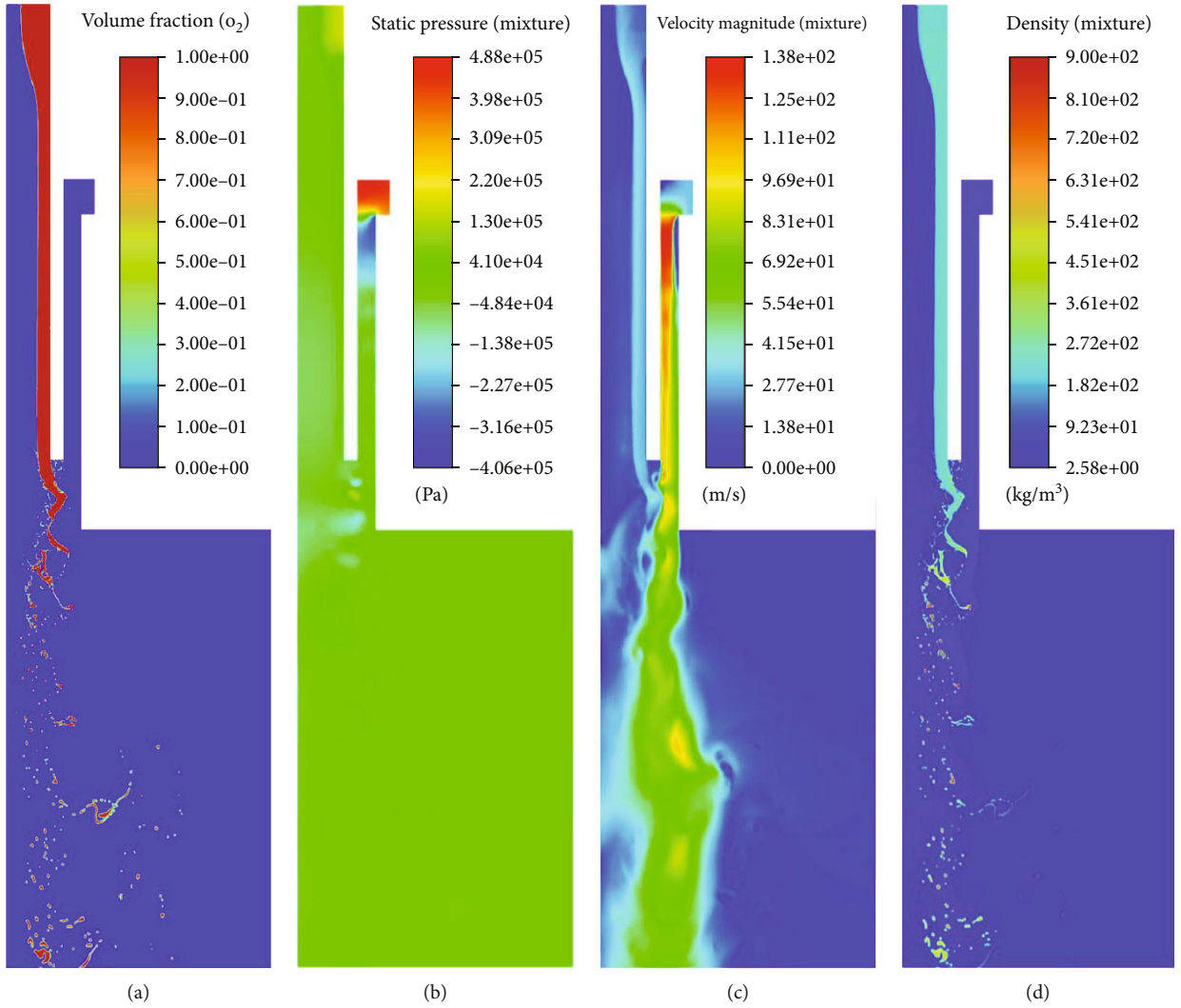

FIGURE 5: Contours of flow field of the injector: (a) volume fraction contour of LOX; (b) pressure contour; (c) velocity contour; (d) density contour.

The following equation defines the compressibility of the gas:

$$Z = \frac{\mathrm{PV}}{\mathrm{RT}} = \frac{V}{V-b} - \frac{aV/\mathrm{RT}}{V^2 + 2bV - b^2}. \tag{7}$$

The parameters a and b are determined by the components using the simple mixing law:

$$\begin{aligned} a &= \sum_{i=1}^{N}\sum_{j=1}^{N} X_i X_j \sqrt{a_i a_j}, \\ b &= \sum_{i=1}^{N} X_i b_i, \end{aligned} \tag{8}$$

where N is the number of components in the mixture. The pure component parameters can be obtained using a relationship with the Peng-Robinson constant, which are shown as follows:

$$\begin{aligned} a_i &= \left(0.457247\frac{R^2 T_{c,i}^2}{p_{c,i}}\right) \\ &\quad \cdot \left[1 + \left(0.37464 + 1.54226\omega_i - 0.26992\omega_i^2\right)\left(1 - \left(\frac{T}{T_{c,i}}\right)^{1/2}\right)\right]^2, \\ b_i &= 0.07780\frac{\mathrm{RT}_{c,i}}{P_{c,i}}, \end{aligned} \tag{9}$$

where $T_{c,j}$ is the critical temperature, $p_{c,j}$ is the critical pressure, and ω_i is the eccentricity coefficient of the i-th component. The PR equation of state is obtained on the basis of the improved Soave-Redlich-Kwong (SRK) equation. The accuracy is higher compared to the Redlich-Kwong (RK) model and SRK model [31]. Therefore, the PR real gas equation of state model is used in this paper for numerical simulation.

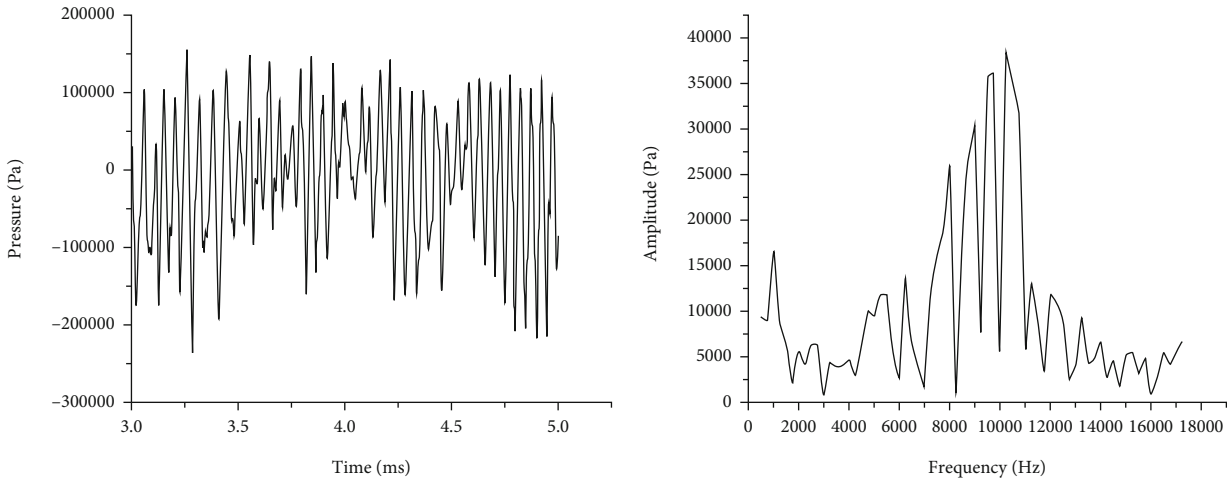

(a)

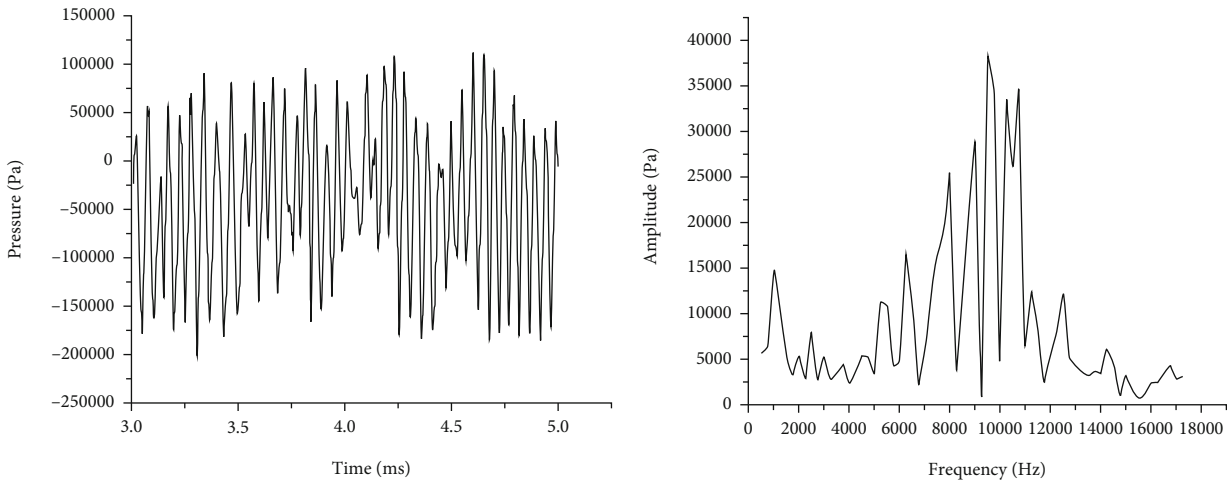

(b)

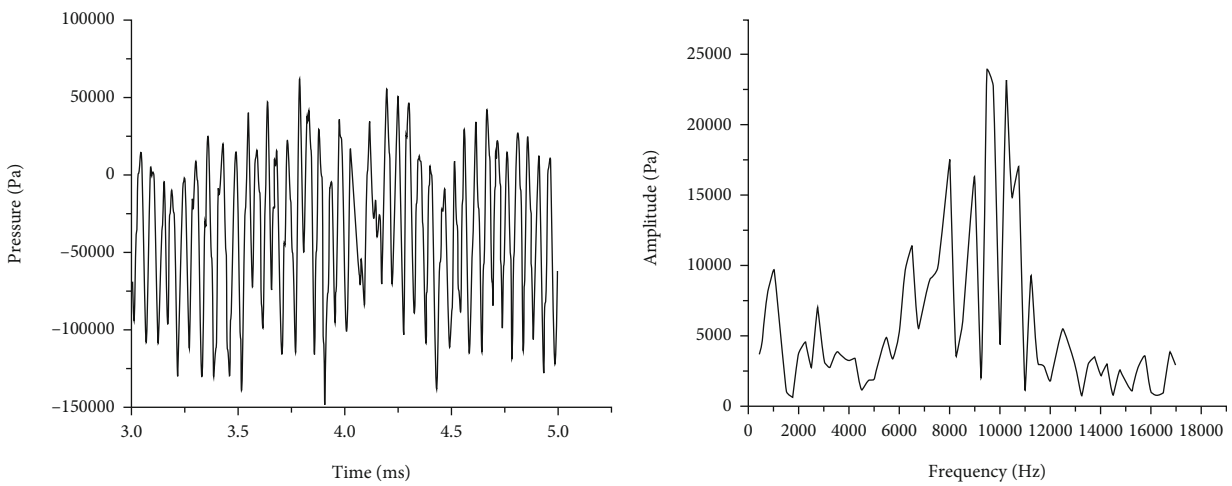

(c)

Figure 6: Continued.

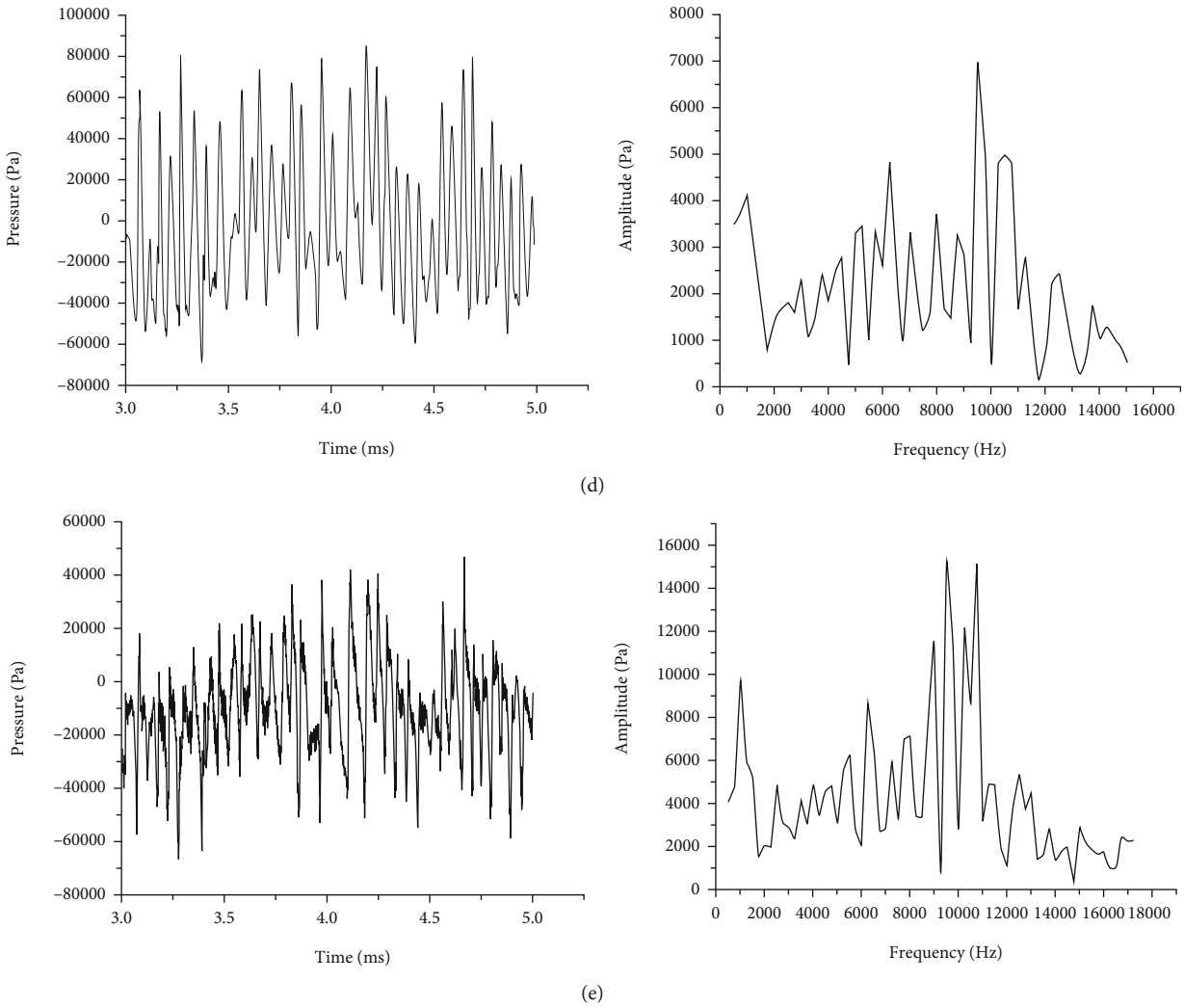

Figure 6: The pressure-time trace and the frequency spectrum of pressure at different monitoring probes of the recess region: (a) probe A; (b) probe B; (c) probe C; (d) probe D; (e) probe E.

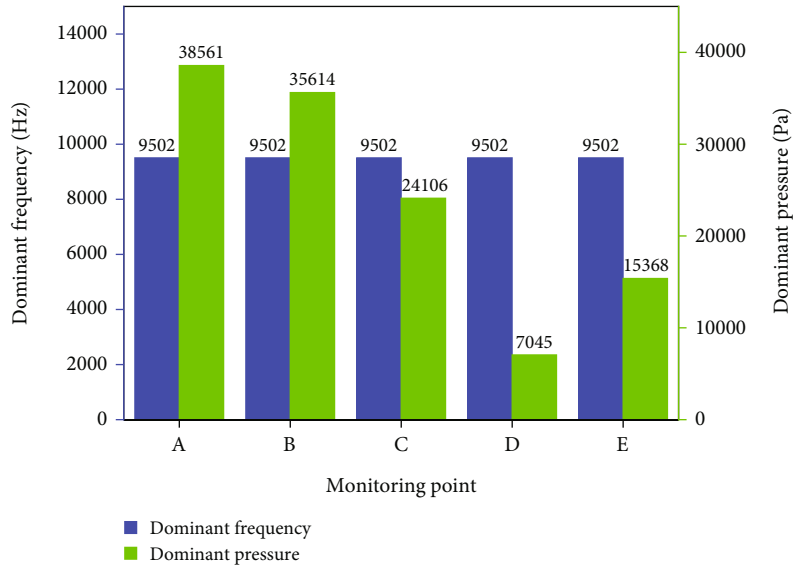

Figure 7: The dominant frequency of pressure oscillation and their dominant pressure at different monitoring probes of the recess region.

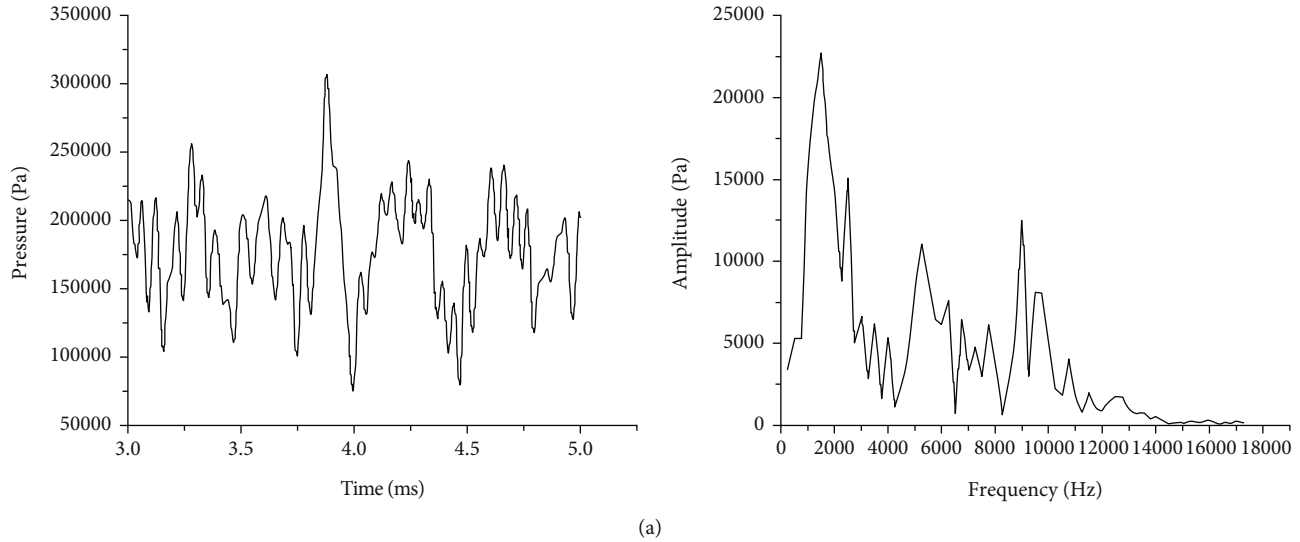

(a)

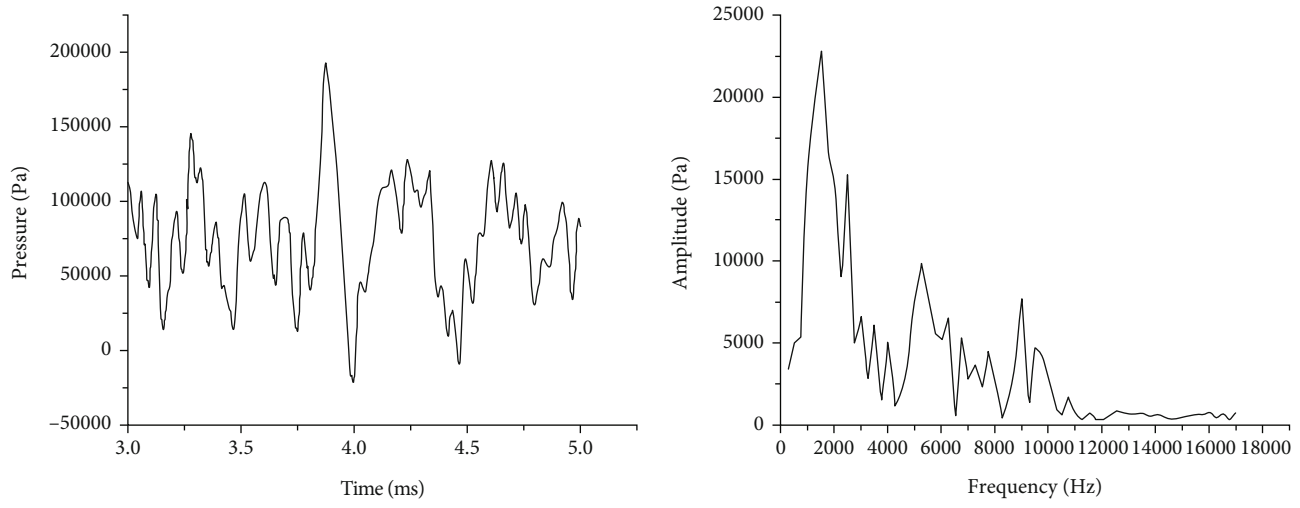

(b)

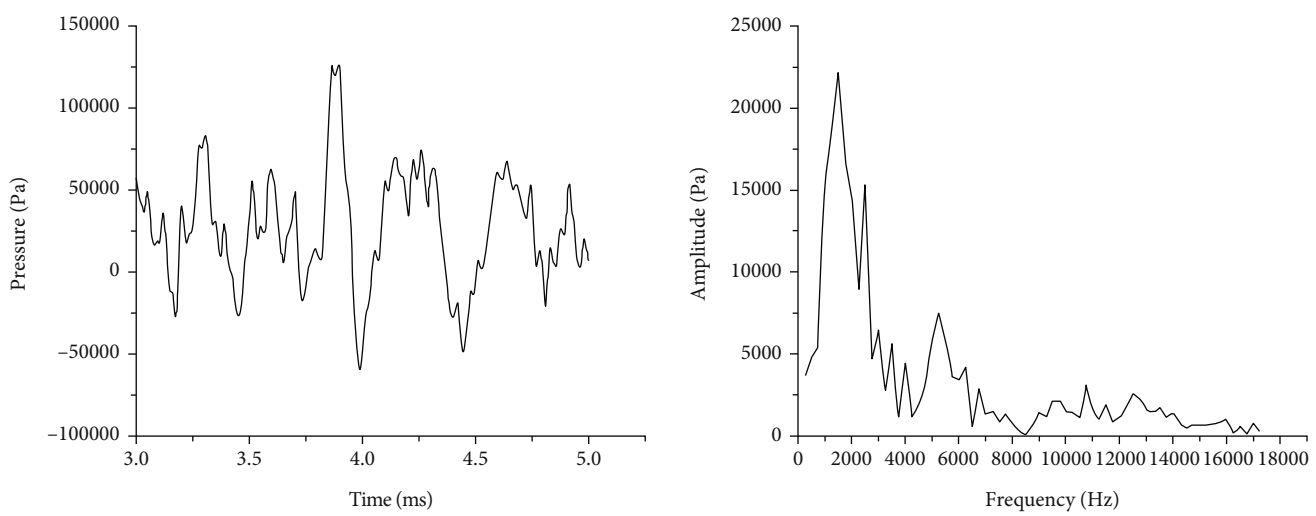

(c)

Figure 8: Continued.

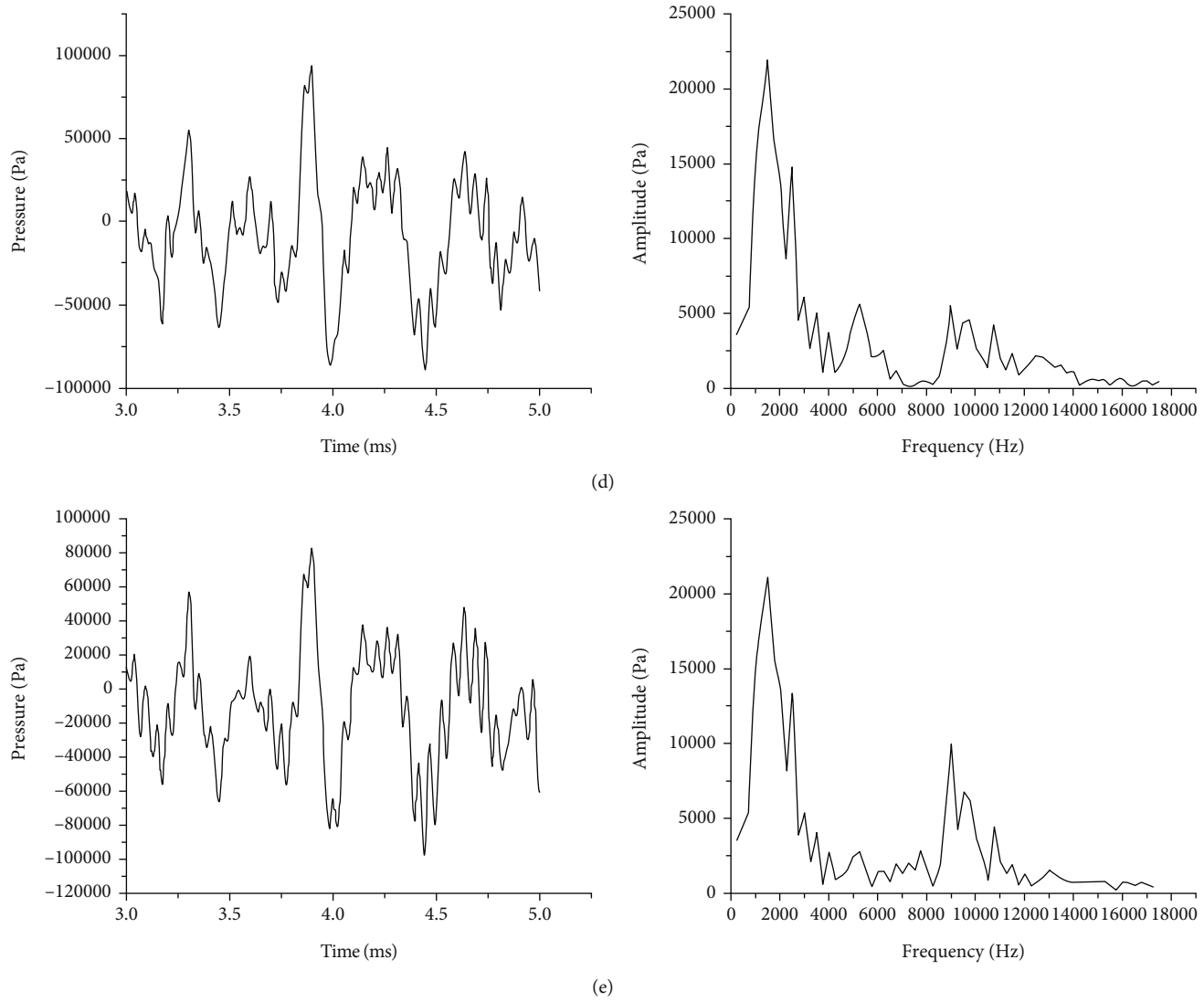

Figure 8: The pressure-time trace and the frequency spectrum of pressure at different monitoring probes of the LOX path: (a) probe F; (b) probe G; (c) probe H; (d) probe I; (e) probe J.

2.3. Numerical Scheme and Accuracy Verification

2.3.1. Computing Domain and Numerical Method. When self-pulsation phenomenon occurs in the gas-liquid swirl coaxial injector, there will be a strong gas-liquid interaction in the recess region. The distribution of gas-liquid phases and the pressure gradient in the flow field are constantly changing. Therefore, a high density of grid is required in the numerical simulation to ensure the accuracy of the calculation, so as to capture the detailed flow field structure characteristics inside and outside the injector during the self-pulsation process. In the simulations of this paper, the physical state of the real fluid of the liquid oxygen/gas hydrogen propellant under the extreme operating conditions in the hot-fire test experiments is considered. In order to meet the computational requirements and shorten the computation time, an axisymmetric two-dimensional computing domain is adopted here for numerical simulation. The computing domain consists of the internal area of the inner swirl injector, the area of gas annular slit, the recess region, and the external flow area downstream of the injector. The structure of hydrogen-collecting cavity part is retained. The structure of oxygen-collecting cavity and the tangential inlet of oxygen in the inner injector are simplified. The schematic diagram is shown in Figure 2. To capture the oscillation information, a variety of monitoring probes were set inside the computing domain. Probe points A~E are located at the recess region of the injector. The liquid path takes the probe points F~J, and the gas path takes the probe points K~N.

Firstly, the model of computing domain of the LOX/GH_2 injector is meshed with a global structure-grid size of 0.045 mm. In order to increase the computational accuracy, the grids in the recess region are encrypted by employing an adaptive structured mesh refinement method. The refined grid size is 0.03 mm, and the growth rate is 1.1. In addition, boundary layers are created at the wall surface, and the mesh transition is ensured to be uniform. The size of the first boundary layer is set to 0.015 mm, and the growth

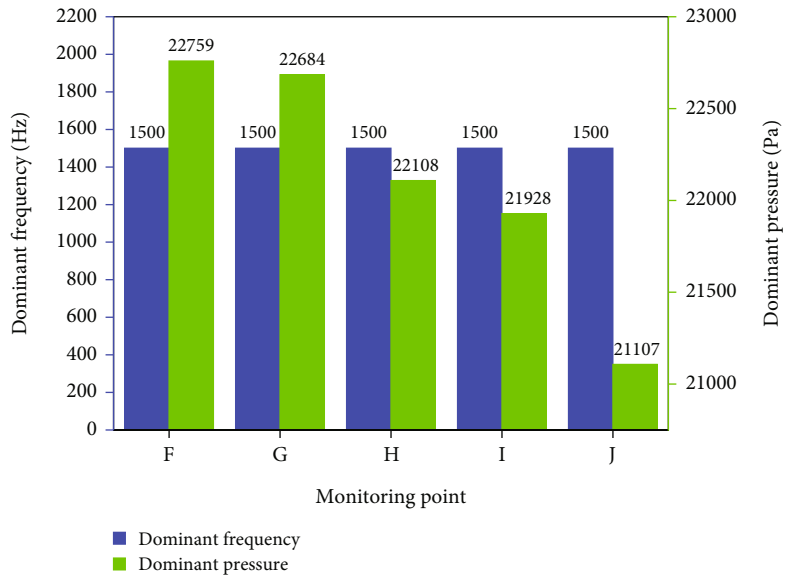

Figure 9: The dominant frequency of pressure oscillation and their dominant pressure at different monitoring probes of the LOX path.

rate is 1.15. In total, 8 boundary layers were generated. The total number of initial grids generated is 336570.

In the simulation, the four tangential holes of the inner injector are simplified to a line in the two-dimensional computing domain. According to the structural and operating parameters in Tables 1 and 2, the radial velocity of the LOX inlet can be solved by

$$v_r = \frac{\dot{m}_l}{\rho \pi D_1 D_{t1}}. \tag{10}$$

The tangential velocity can be solved by

$$v_t = \frac{\dot{m}_l}{\rho \pi D_{t1}^2}, \tag{11}$$

where D_1 and D_{t1} are the diameter of the swirl chamber and the diameter of the tangential hole of the inner injector, respectively. In the Fluent solver, the velocity-inlet boundary condition was set at the LOX inlet. The mass flow-inlet boundary condition was used for the GH_2 inlet. The outlet was set as the pressure-outlet boundary condition. The center axis of the injector was an axisymmetric boundary condition. The other boundaries adopted nonslip wall conditions. The operating conditions for the injector and the ambient conditions of combustion chamber were set according to the parameters listed in Table 2.

The RNG $k-\varepsilon$ turbulence model was used to calculate the strong cyclonic flow process in the gas-liquid coaxial injector. The VOF model was adopted to capture the interface of the gas-liquid two-phase flow, where liquid oxygen is the main phase and gaseous hydrogen is the secondary phase. The energy equation was considered, and the PR equation of state was used to ensure the accuracy of the calculation for the supercritical operating conditions. Moreover, a pressure-based solver was used for transient calculations. The symmetry of the model is rotational symmetry. The solution method adopted the pressure-implicit with splitting of operators (PISO) algorithm [13, 32]. Considering the size of the grids, the iteration step length was selected as 5×10^{-7} s, and the number of iteration steps was 8000.

2.3.2. Grid Independence Study. The grid-independence verification is performed with the given operating conditions. Using the same meshing method, three sets of grid systems for the computational model were created by adjusting the global grid size. These three grid systems were the coarse grid (260 thousand cells), the intermediate grid (330 thousand cells), and the fine grid (400 thousand cells), respectively. The self-pulsation process of the LOX/GH_2 injector was simulated on these grids. The oscillation frequency of the pressure at a point in the recess region during self-pulsation is chosen as the criterion for discriminating the grid independence. Figure 3 displays the self-pulsation frequencies (i.e., the frequencies of pressure oscillations in the recess chamber [33]) obtained by the fast Fourier transform (FFT) of pressure-time trace. The dominant frequencies of pressure oscillations calculated from the three grid systems are 10714 Hz, 11806 Hz, and 11882 Hz, respectively. The difference between the dominant frequencies from the coarse and the intermediate grids is 9.1%. The difference between the dominant frequencies from the intermediate and the fine grids is only 0.64%. At this point, it can be considered that the calculated results are convergent and independent of the number of the grid cell. Thus, given the computing cost and simulation accuracy, the intermediate grid system was adopted for the present study.

2.3.3. Validation of Experimental Data. To verify the accuracy of the numerical simulation method, the frequency spectrum of pressure oscillation at the recess region of the injector, calculated under the intermediate grid system, was

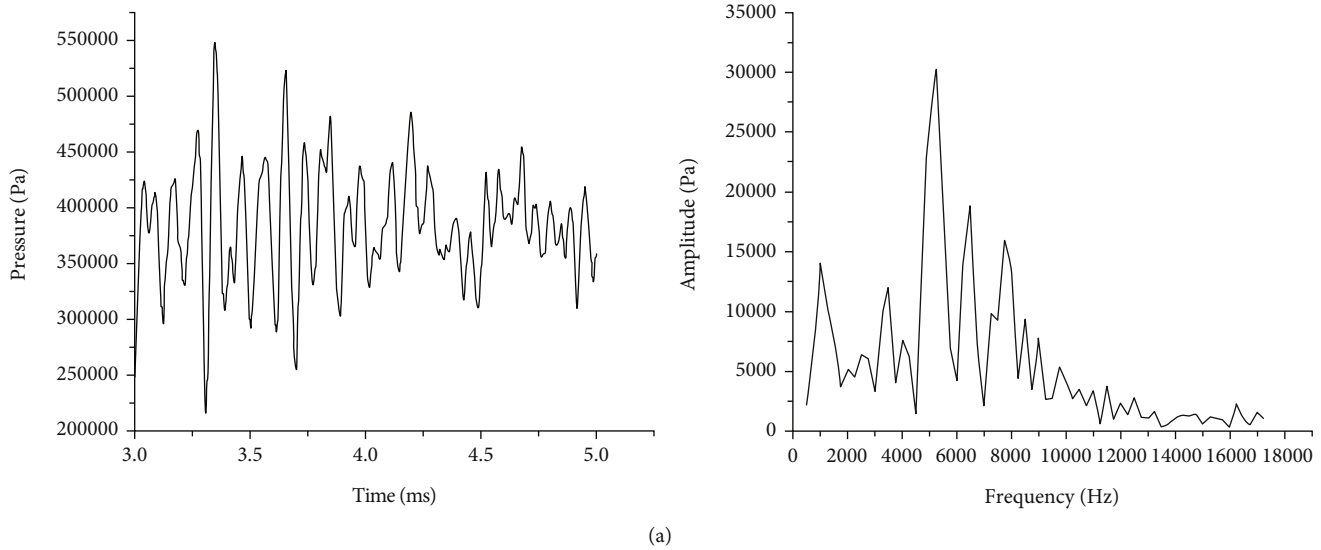

(a)

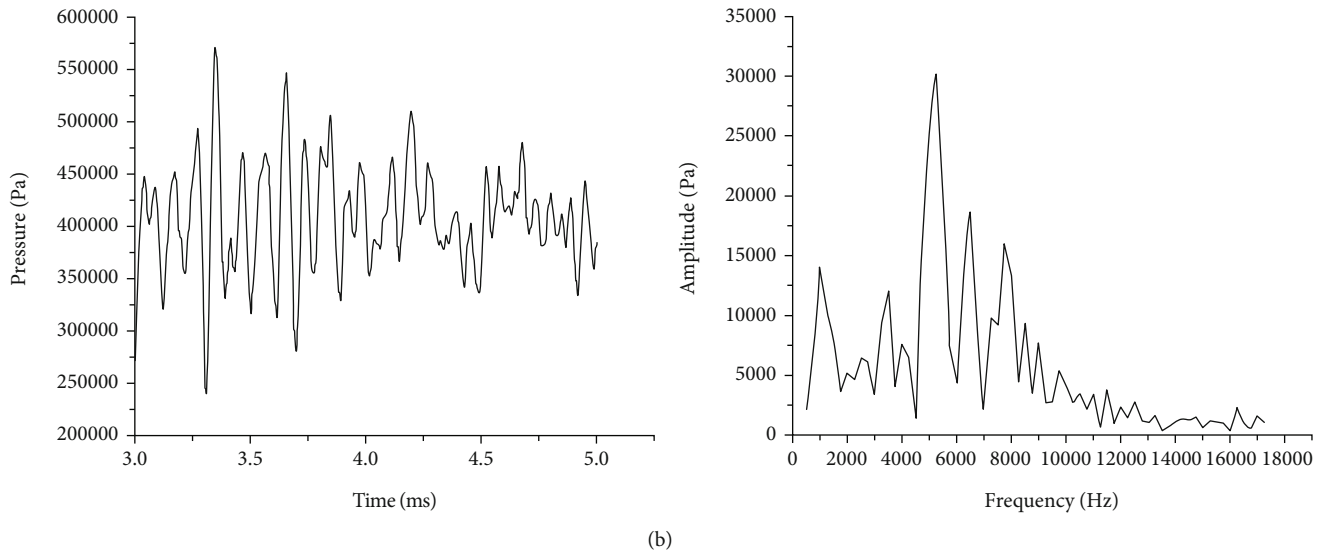

(b)

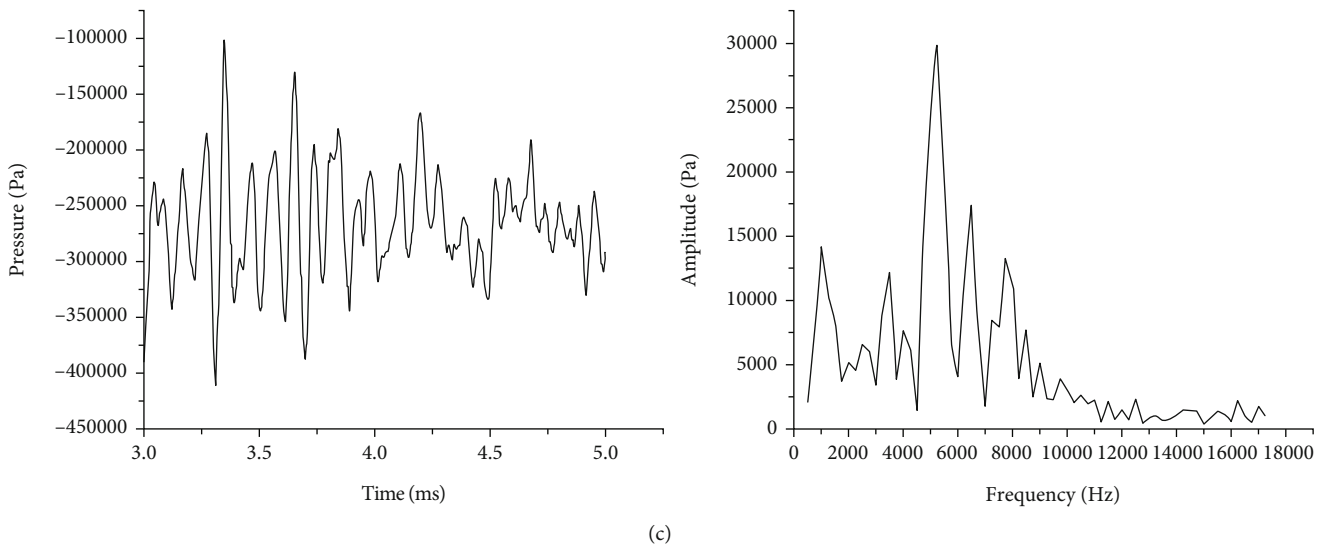

(c)

Figure 10: Continued.

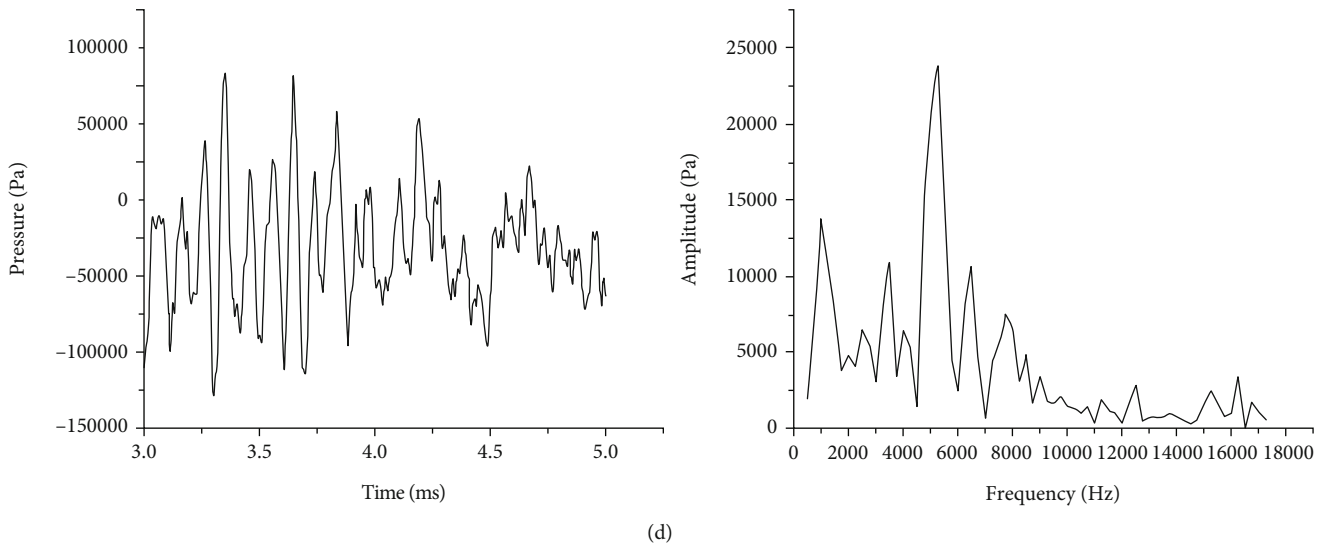

Figure 10: The pressure-time trace and the frequency spectrum of pressure at different monitoring probes of the GH_2 path: (a) probe K; (b) probe L; (c) probe M; (d) probe N.

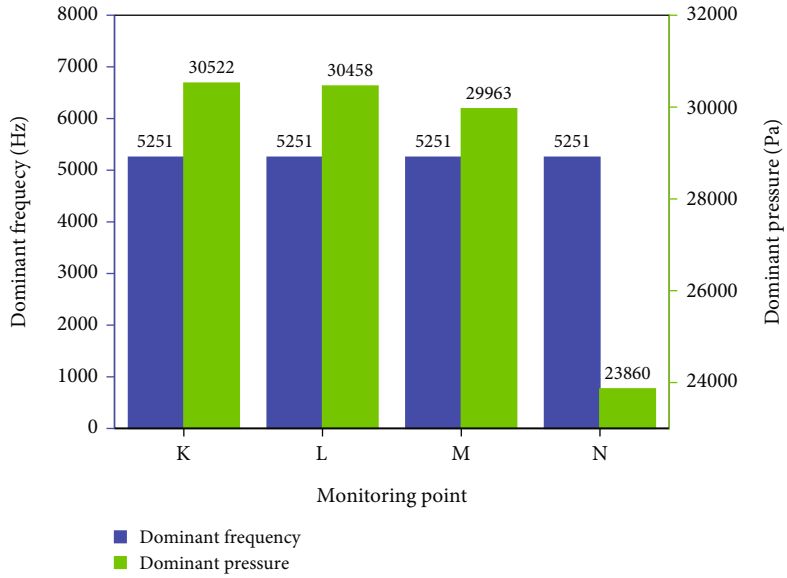

Figure 11: The dominant frequency of pressure oscillation and their dominant pressure at different monitoring probes of the GH_2 path.

Table 3: The operating conditions that vary the flow rate of GH_2 for the simulation.

Group	1	2	3	4	5
Flow rate of LOX $\dot{m}_l$ (g/s)	134	134	134	134	134
Flow rate of $GH_2\dot{m}_g$ (g/s)	130	143	161	183	212
LOX/GH_2 mixing ratio	1.03	0.93	0.83	0.73	0.63
Excess oxygen coefficient	0.128	0.116	0.104	0.091	0.078

compared with the experimental data. The experimental data are the pressure oscillations measured at the oxygen-collecting cavity of the same injector in reference [24] under the same operating conditions in the hot-fire test. As shown in Figure 4, the dominant frequency of the pressure oscillation present in the injector during the hot test experiment was about 10632 Hz. The dominant frequency of the pressure oscillation in the injector recess region was calculated numerically to be 11806 Hz. The difference between them is 11.04%. At the peak of the pressure oscillation and before reaching the peak, the pressure values during the hot test are higher than the simulated results. The experimental pressure peak (7250 Pa) is 10.69% larger than the simulated pressure peak (6550 Pa). The main reason for these differences is that the dominant frequency of pressure oscillations in the simulation is calculated from the axisymmetric two-dimensional computing domain. In addition, the computing domain established by the numerical simulation simplifies the structures of the tangential holes and oxygen-collecting cavity in the LOX/GH_2 injector. Therefore, the values of pressure oscillations generated in the simulation are reduced.

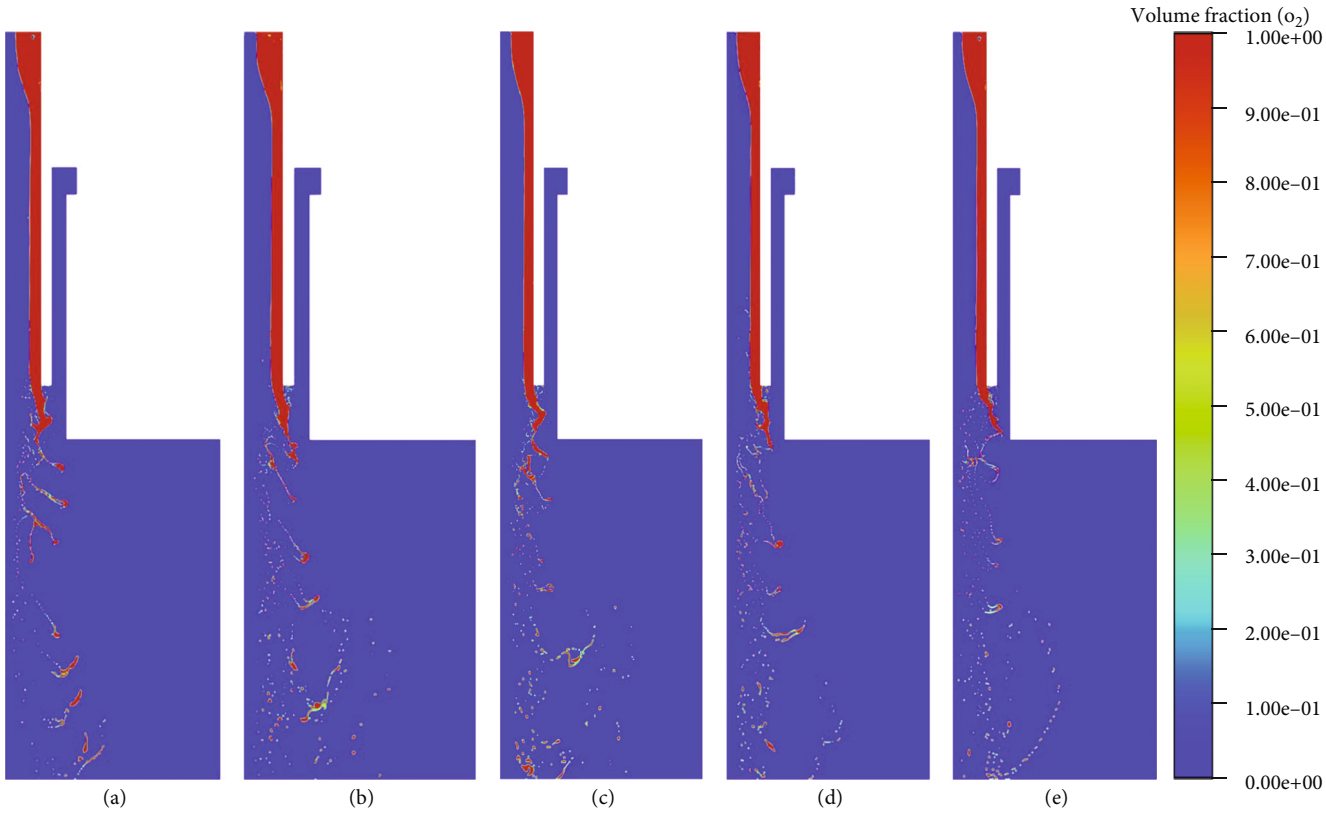

Figure 12: The contours of oxygen volume fraction under different flow rates of GH_2: (a) $\dot{m}_g = 130$ g/s; (b) $\dot{m}_g = 143$ g/s; (c) $\dot{m}_g = 161$ g/s; (d) $\dot{m}_g = 183$ g/s; (e) $\dot{m}_g = 212$ g/s.

The errors in the dominant frequency and amplitude of the pressure obtained from the simulation and experiment are within acceptable range. And seen from the change trend of pressure oscillation, the simulated and experimental results are in good agreement. This indicates that the accuracy of the numerical model of the injector developed in this study is high enough to carry out the following study of the self-pulsation characteristics.

3. Results and Discussion

3.1. Self-Pulsation Mechanism and Analysis of Amplitude-Frequency Characteristics

3.1.1. Analysis of the Self-Pulsation Mechanism. According to the numerical model and method established above, the calculated results of the internal and external flow fields of the LOX/GH_2 swirl coaxial injector are shown in Figure 5, which are, respectively, the volume fraction contour of LOX, pressure contour, velocity contour, and density contour for the full flow field. The pressure in the pressure contour is the gauge pressure, and the initial pressure (i.e., ambient pressure) of the external flow field of the injector is 8.68 MPa. From the volume fraction contour of LOX (Figure 5(a)) and the density contour (Figure 5(d)), it can be seen that the thickness of liquid oxygen film is large at the injector inlet but then decays rapidly. The film thickness basically does not change until it reaches the recess region. At the recess region, the liquid oxygen film is destabilized and oscillated by the action of the annular slit gas. Then, it is broken under the action of gas-liquid shear force to form liquid filaments and liquid lumps, which are further broken downstream to form numerous small liquid droplets. Analysis of Figures 5(b) and 5(c) shows that the pressures at the LOX and GH_2 inlets are relatively high. At the annular slit inlet of GH_2, the velocity of hydrogen flow increases due to the sudden decrease of the flow area, resulting in a decrease of the pressure at this position. At the recess region, the liquid film oscillates and breaks up periodically due to the shearing and entraining effects of the gas on the liquid phase. There are high-pressure point and low-pressure point in this vicinity.

At the recess region of the injector, the periodic self-pulsation phenomenon can be explained by two factors: the centrifugal force of the conical liquid sheet and the resistance of the gas flow from the annular slit. When the centrifugal liquid film flows into the recess region from the inner injector, the tangential velocity of the liquid film is gradually converted into radial velocity. At this time, the centrifugal force of the liquid film is greater than the resistance of the annular gas flow, and the liquid sheet expands toward the wall of the recess chamber. Then, the resistance of the annular gas flow to the liquid film will increase, resulting in a higher pressure. When the centrifugal force of the liquid sheet is balanced with the resistance of the annular gas flow, the liquid sheet continues to move toward the wall of the recess chamber due to the inertia. The resistance of the

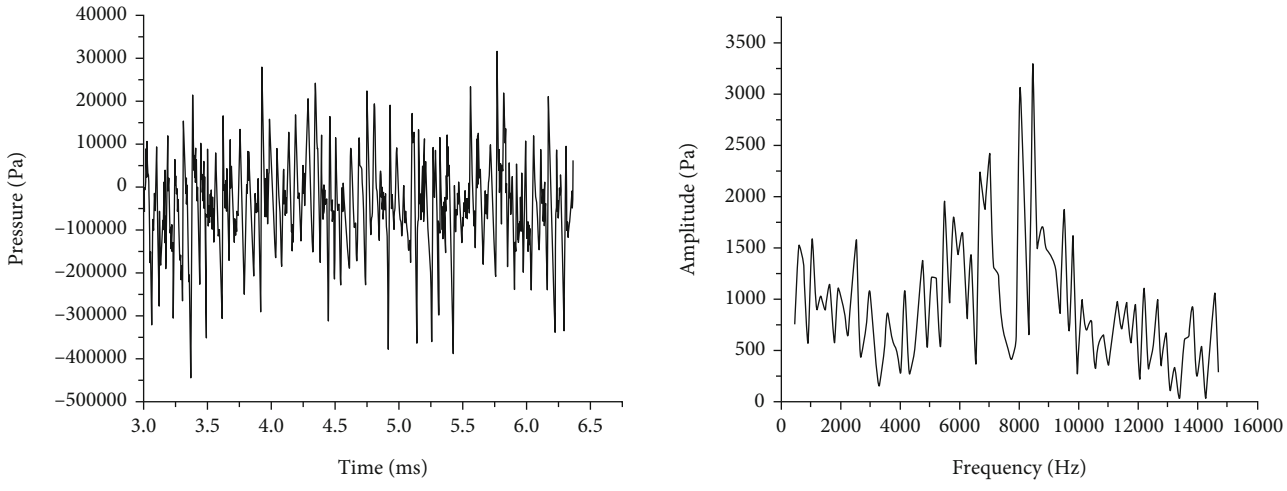

(a)

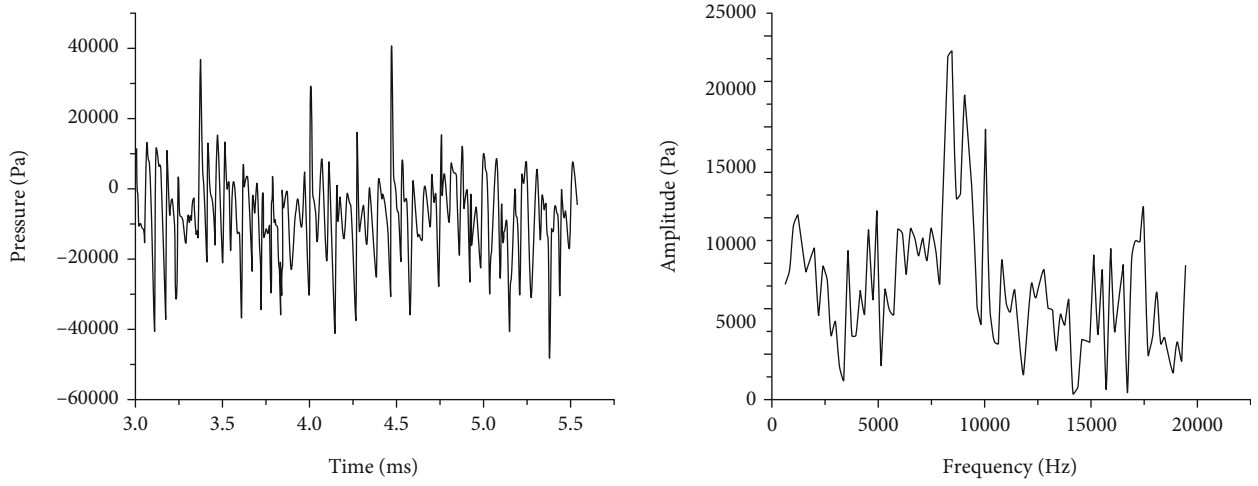

(b)

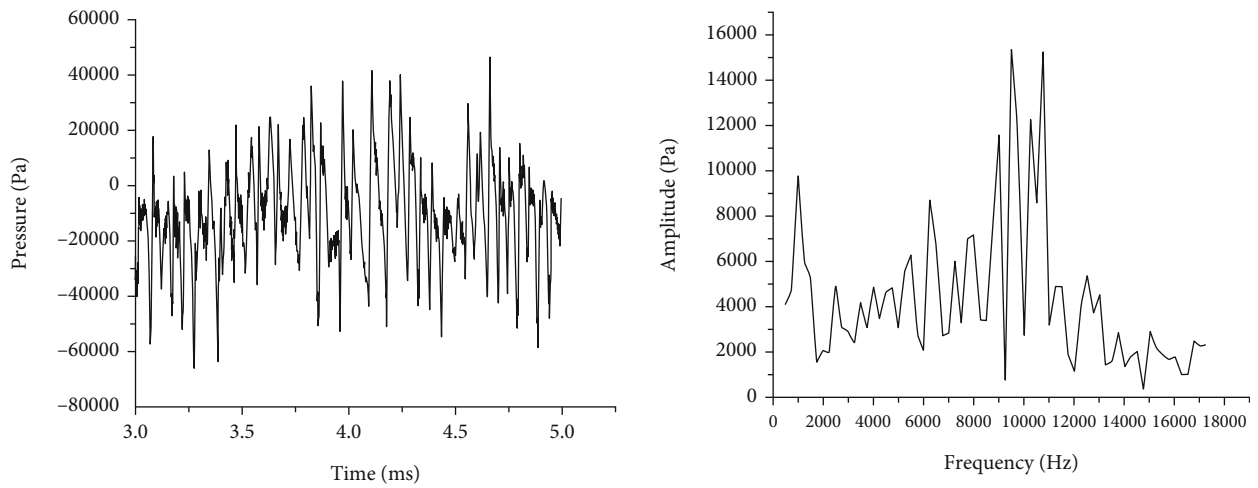

(c)

Figure 13: Continued.

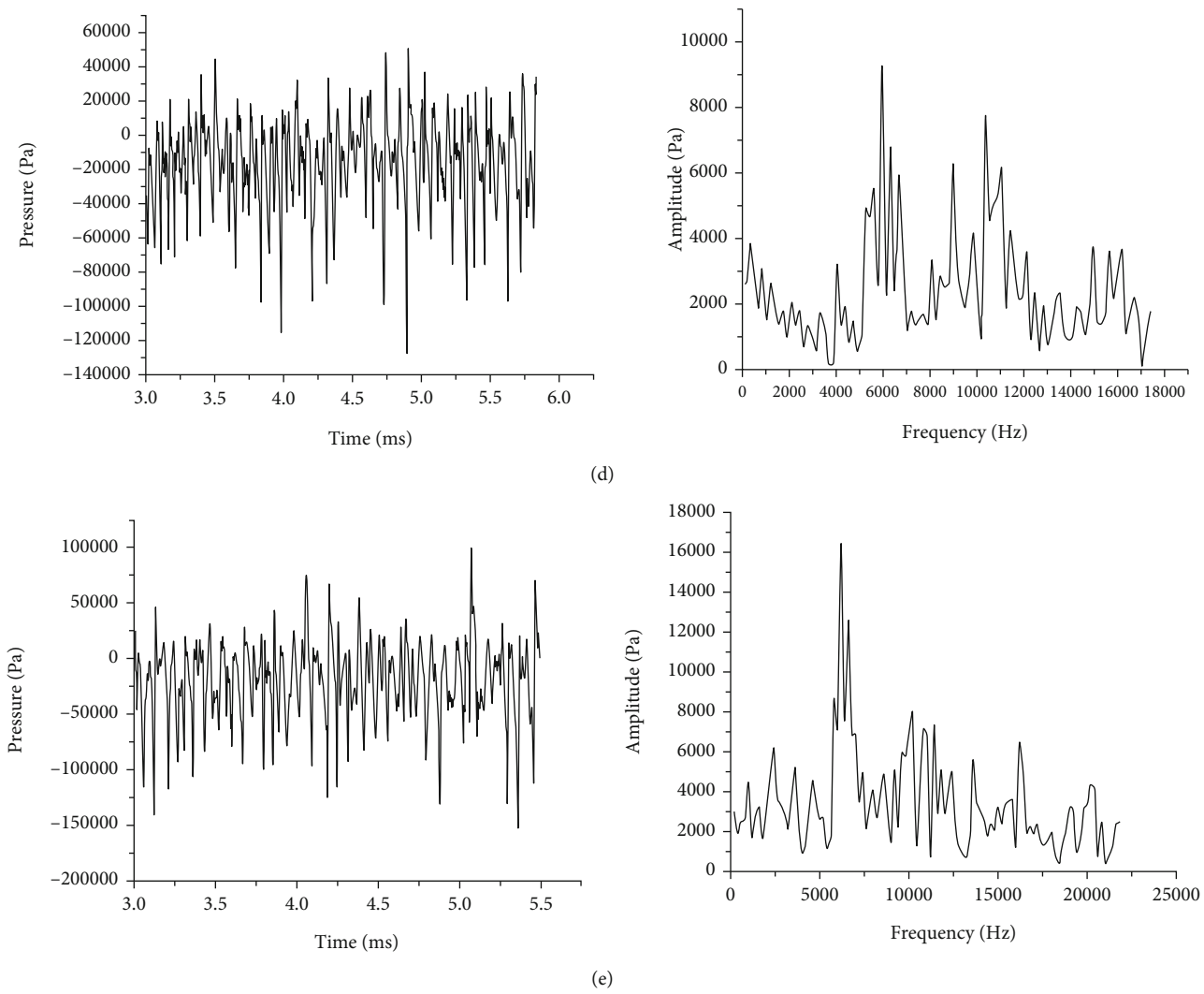

FIGURE 13: The pressure-time trace and frequency spectrum of pressure under different flow rates of GH_2: (a) $\dot{m}_g = 130$ g/s; (b) $\dot{m}_g = 143$ g/s; (c) $\dot{m}_g = 161$ g/s; (d) $\dot{m}_g = 183$ g/s; (e) $\dot{m}_g = 212$ g/s.

annular gas flow to the liquid sheet is further increased, resulting in a further increase in pressure. When the outward expansion speed of liquid sheet decreases to zero, the pressure in the blocked region of the recess region reaches the maximum. At this point, the resistance from the annular gas flow is greater than the centrifugal force of the liquid sheet. Therefore, the liquid sheet contracts toward the center, and the blockage region is opened, resulting in a rapid decrease in pressure. After that, the continuous flow of the liquid film starts the next cycle of self-pulsation oscillation at the recess region.

3.1.2. Amplitude-Frequency Characteristics of Recess Region. Many studies have shown that the recess region of the liquid-centered swirl coaxial injector is an important factor affecting the occurrence of self-pulsation, so the amplitude-frequency characteristics of the recess region are first analyzed here. Five monitoring probes were set up in the recess region, which is depicted in Figure 2. The pressure-time curve and the frequency spectrum of pressure at different probes of the recess region are calculated and shown in Figure 6. Moreover, the dominant frequencies of pressure oscillations at the five probes and their dominant pressures (i.e., the pressure corresponding to the dominant frequency) are extracted from this figure, as shown in Figure 7.

According to Figures 6 and 7, the dominant frequencies of pressure oscillations at the five probes of A~E are all 9502 Hz, which means that the dominant frequencies of pressure oscillations at different observation points in the recess region are the same when self-pulsation occurs. Therefore, the selection of the location of the monitoring probes in the recess region has little influence on the correct extraction of the dominant frequency of the oscillation.

From the pressure-time traces of each monitoring probe, it can be found that the pressure of all monitoring points at the recess region basically shows periodic oscillations. This is because the centrifugal liquid sheet periodically blocks the annular gas path at the recess region, which causes periodic oscillation and disturbance of the liquid sheet, then resulting in periodic pulsation of the pressure. In addition, although

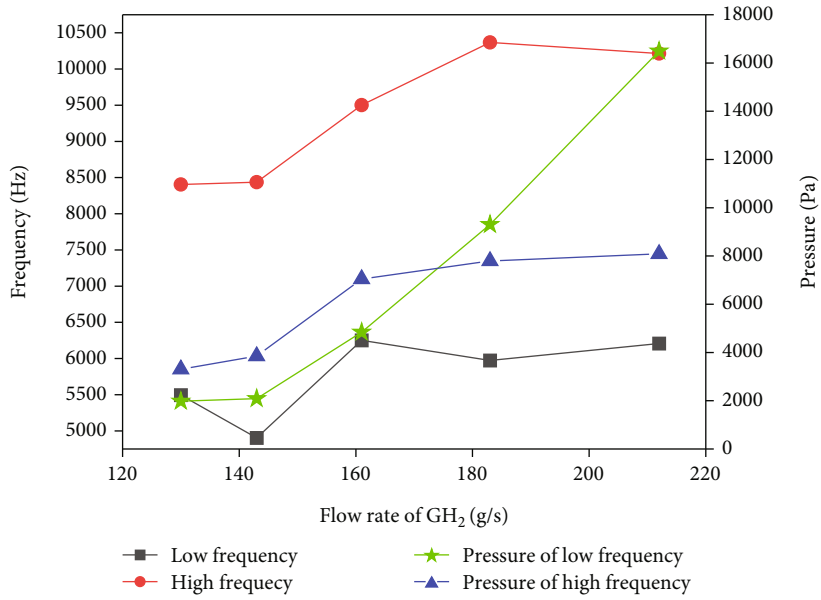

Figure 14: High/low frequencies of pressure oscillations under different flow rates of GH_2 and their corresponding pressure.

Table 4: The operating conditions that vary the flow rate of LOX for the simulation.

Group	1	2	3	4	5
Flow rate of LOX $\dot{m}_l$ (g/s)	101	117	134	149	165
Flow rate of GH_2 $\dot{m}_g$ (g/s)	161	161	161	161	161
LOX/GH_2 mixing ratio	0.63	0.73	0.83	0.93	1.03
Excess oxygen coefficient	0.078	0.091	0.104	0.116	0.128

the dominant frequency of pressure oscillation is the same at different monitoring probes, the corresponding dominant pressure for the frequency varies greatly. Comparing the dominant pressures of monitoring points A, B, and C, it can be known that the dominant pressure of probe A > the dominant pressure of probe B > the dominant pressure of probe C. That is to say, in the recess region, the closer to the downstream position, the lower the dominant pressure is, which is consistent with the information shown in the pressure contour in Figure 5(b). Comparing the dominant pressure at the four monitoring points of B, E, C, and D, it can be seen that the dominant pressure of probe B > the dominant pressure of probe E, and the dominant pressure of probe C > the dominant pressure of probe D. That is, in the recess region, the closer to the position of the gas annular slit is, the lower the dominant pressure is. This results from the larger gas flow rate from the annular slit, which causes the pressure in this area to decrease.

3.1.3. Amplitude-Frequency Characteristics of LOX Path. Five monitoring probes F~J were selected upstream of the LOX path (i.e., liquid channel) of the injector, as shown in Figure 2. It is used to explore whether the injector would cause the upstream LOX path to also oscillate in pressure or flow when the self-pulsation occurs, as well as the amplitude-frequency characteristics here. The pressure-time trace and the frequency spectrum of pressure at different monitoring points of the upstream LOX path are calculated and shown in Figure 8. The dominant frequencies of pressure oscillations at these five points and their corresponding dominant pressures were extracted from this figure, as shown in Figure 9.

According to Figures 8 and 9, the oscillation trend of the pressure with time and the amplitude-frequency characteristic curve at the five probes of F~J are basically the same. The dominant frequency of pressure oscillation at each point is 1500 Hz, which indicates that the oscillation frequency at each point in the upstream region of the LOX path is basically the same. As the monitoring point moves downstream along the LOX path, the corresponding dominant pressure value decreases. However, the decrease in the dominant pressure was small, with only a 7.83% change from point F to point J.

3.1.4. Amplitude-Frequency Characteristics of GH_2 Path. Four monitoring probes K~N were selected upstream of the GH_2 path (i.e., gas channel) of the injector, as shown in Figure 2. It is used to explore whether the injector would cause the upstream GH_2 path to also oscillate in pressure or flow when the self-pulsation occurs, as well as the amplitude-frequency characteristics here. The pressure-time trace and the frequency spectrum of pressure at different monitoring points of the upstream GH_2 path are calculated and shown in Figure 10. The dominant frequencies of pressure oscillations at these four points and their corresponding dominant pressures were extracted from this figure, as shown in Figure 11.

According to Figures 10 and 11, the oscillation trend of the pressure with time and the amplitude-frequency characteristic curve at the four probes of K~N are basically the same. The dominant frequency of pressure oscillation at each point is 5251 Hz, i.e., the oscillation frequency at each

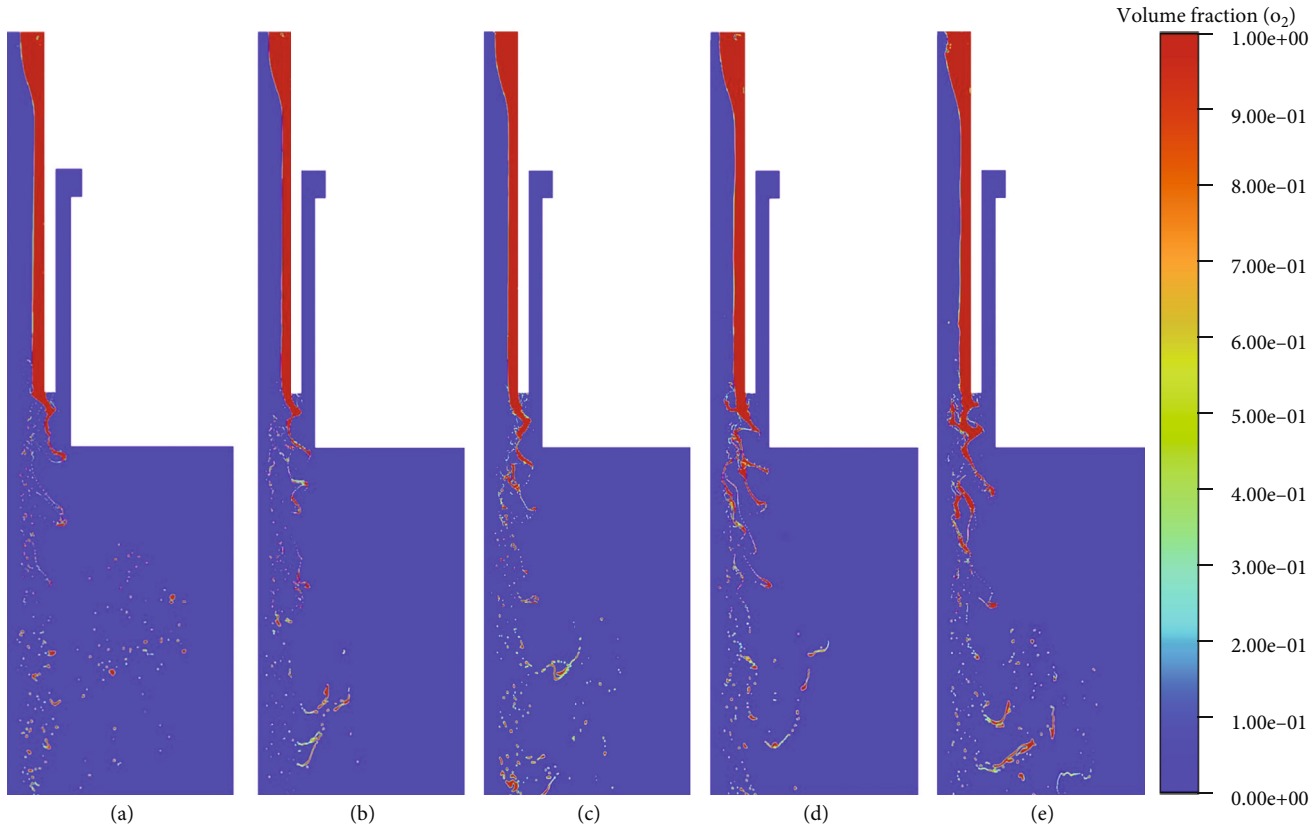

FIGURE 15: The contours of oxygen volume fraction under different flow rates of LOX: (a) $\dot{m}_l = 101$ g/s; (b) $\dot{m}_l = 117$ g/s; (c) $\dot{m}_l = 134$ g/s; (d) $\dot{m}_l = 149$ g/s; (e) $\dot{m}_l = 165$ g/s.

point in the upstream region of the gas annular slit is basically the same. As the monitoring point moves downstream along the GH_2 path, the corresponding dominant pressure decreases. At first, the decrement of the dominant pressure was very small, with a change of only 1.86% from probe K to probe M. However, the decrement in the dominant pressure from probe M to probe N is significant, with a change of 25.6%.

Combined with the analysis for the recess region and the LOX path above, it can be seen that the dominant frequencies of pressure oscillation in these three different regions (recess region, upstream of the LOX path, and upstream of the GH_2 path) are different when the self-pulsation occurs. However, for the monitoring points in each region, the dominant frequency of pressure oscillation is approximately the same. Therefore, there may be a transition region between these different pressure monitoring regions, and the dominant frequency of pressure oscillation at each point in this transition region should be different.

3.2. Effect of the Operating Conditions on the Self-Pulsation Characteristics

3.2.1. The Effect of the Flow Rate of GH_2. The operating conditions were changed by varying the oxidizer-to-fuel mixing ratio. And the effect of different flow rates of GH_2 on the self-pulsation performance of the injector was investigated first. Referring to the existing hot test experiments, the parameters of operating conditions of the simulation are determined as shown in Table 3. The calculated contours of oxygen volume fraction under different flow rates of GH_2 when the self-pulsation occurs are shown in Figure 12.

According to the contours, it can be seen that the liquid film is already partially broken into droplets at the injector outlet at a higher hydrogen flow rate of 212 g/s. The thickness of the remaining unbroken liquid filament is thin. There is almost no continuous liquid filament downstream of the injector, and the generated droplets are also very small. While the hydrogen flow rate is 183 g/s, the liquid film at the injector outlet just starts to generate droplets. The thickness of liquid film and the distribution of liquid filaments at this point are significantly greater than those at a hydrogen flow rate of 212 g/s. In the downstream, there are some continuous liquid filaments that have not yet broken into droplets. When the hydrogen flow rate is reduced to 161 g/s, there is still a continuous liquid film at the injector outlet. There are also some liquid filaments downstream of the outlet, and the generated droplets are relatively large. When the hydrogen flow rate is 143 g/s, the liquid film thickness at the injector outlet will be larger. And there are more liquid filaments and liquid lumps in the downstream. The droplet size is relatively larger, and the number of droplets is smaller. When the hydrogen flow rate is further reduced to 130 g/s, there are more large liquid filaments and liquid lumps, and fewer small droplets in the downstream. At this point, it can be clearly observed that the self-pulsation

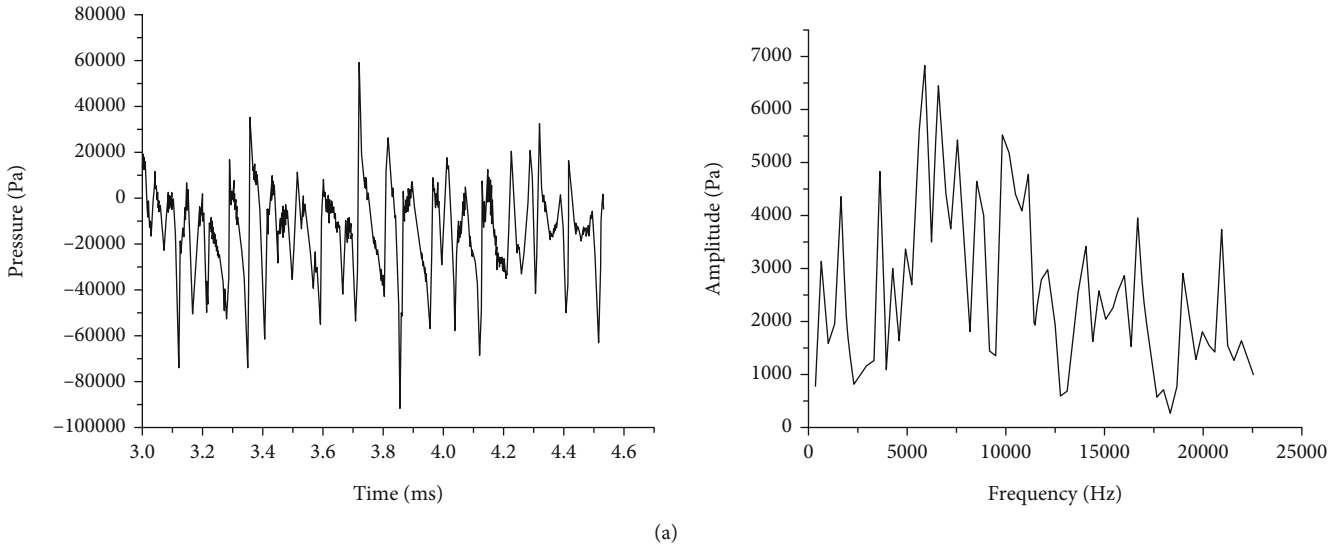

(a)

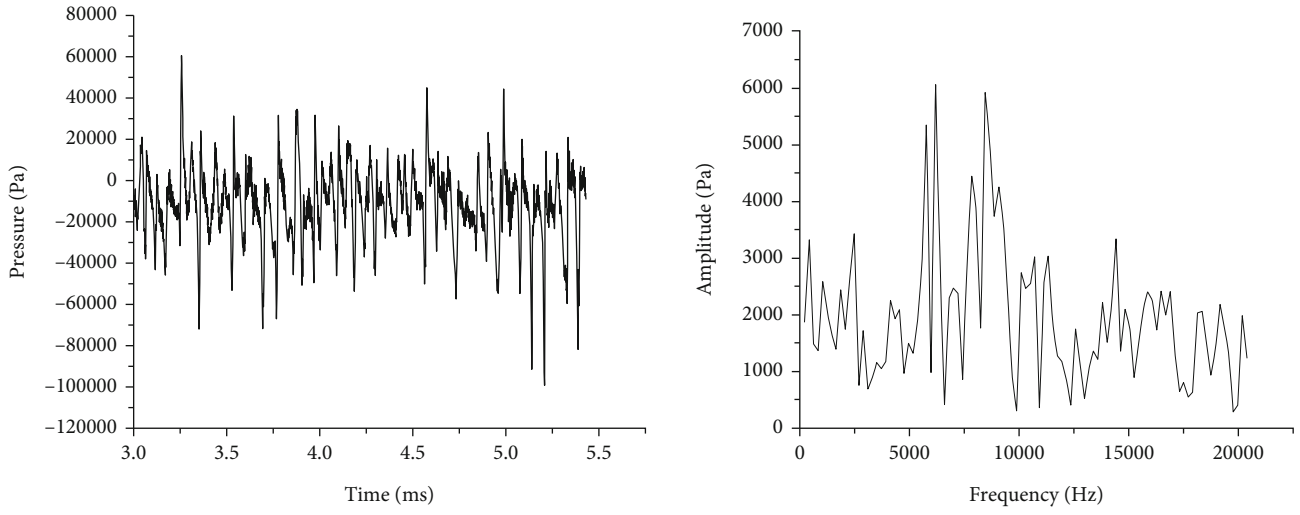

(b)

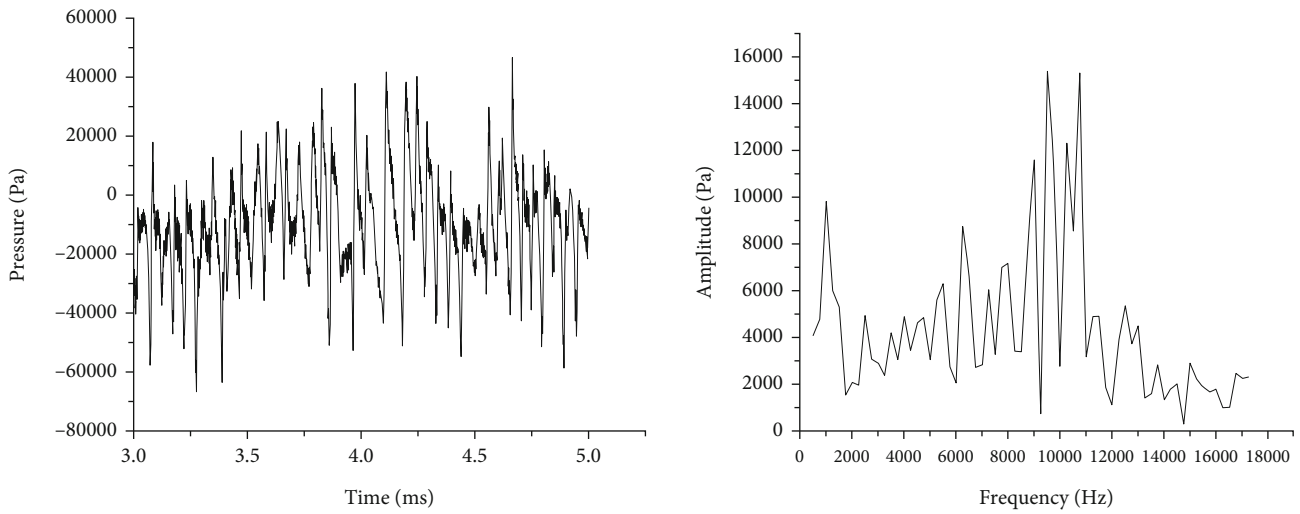

(c)

Figure 16: Continued.

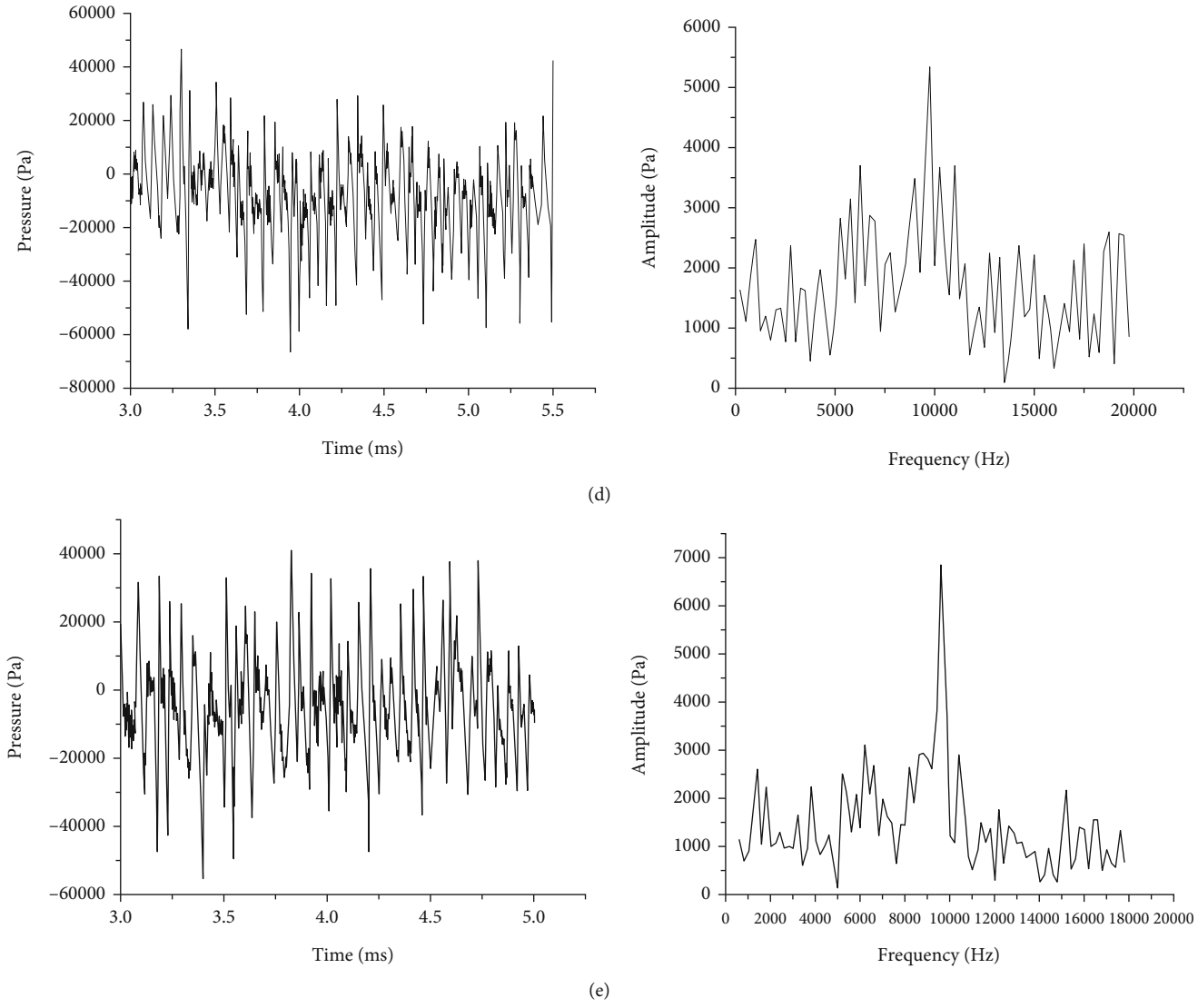

Figure 16: The pressure-time trace and frequency spectrum of pressure under different flow rates of LOX: (a) $\dot{m}_l = 101$ g/s; (b) $\dot{m}_l = 117$ g/s; (c) $\dot{m}_l = 134$ g/s; (d) $\dot{m}_l = 149$ g/s; (e) $\dot{m}_l = 165$ g/s.

oscillation causes the liquid phase present a periodic distribution in space: one strand after another of liquid filaments is continuously ejected from the injector outlet. On the whole, as the flow rate of GH_2 gradually decreases, the shearing force of the gas on the liquid film weakens. The continuity of the liquid film at the recess region becomes better and less likely to break. The position where the liquid filaments generated by the liquid film are massively broken into droplets moves further downstream.

The pressure-time plots and the frequency spectrum of pressure for different flow rate of GH_2 are shown in Figure 13. From the frequency spectrum graphs, it can be seen that for all conditions of different flow rate of GH_2, there are relatively violent pressure amplitudes and oscillations roughly around the oscillation frequencies of 6000 Hz and 10000 Hz. This is especially true for the condition of a higher GH_2 flow rate. For the convenience of summarizing the law, these two oscillation frequencies are defined as low frequency and high frequency of pressure oscillations, respectively. Their corresponding pressures are defined as low-frequency pressure and high-frequency pressure, respectively. The subsequent studies on the effects of the flow rate of LOX and the initial temperature of GH_2 have made similar distinctions and will not be repeated. In this way, the high/low frequencies of pressure oscillation and their corresponding pressures for different flow rates of GH_2 were obtained as drawn in Figure 14.

According to Figure 14, it can be seen that both the low-frequency pressure and the high-frequency pressure decrease during the reduction of the flow rate of GH_2 from 212 g/s to 130 g/s. And the decrease rate of low-frequency pressure is obviously larger than that of high-frequency pressure. When the flow rate of GH_2 is 212 g/s and 183 g/s, the low-frequency pressure is higher than the high-frequency pressure. In these two cases, the dominant frequency of pressure oscillation is around 6000 Hz (Figures 13(d) and 13(e)). For the latter three conditions of lower flow rate of GH_2, the high-frequency pressure is

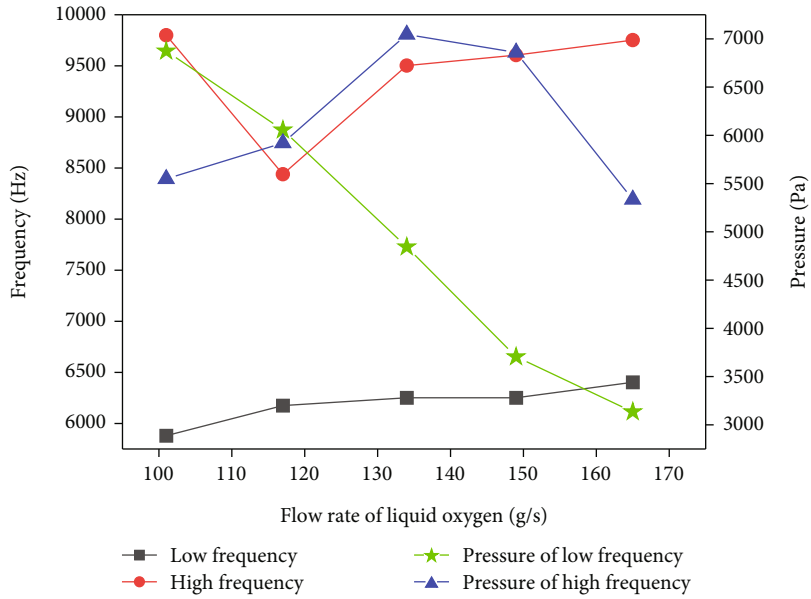

Figure 17: High/low frequencies of pressure oscillations under different flow rates of LOX and their corresponding pressure.

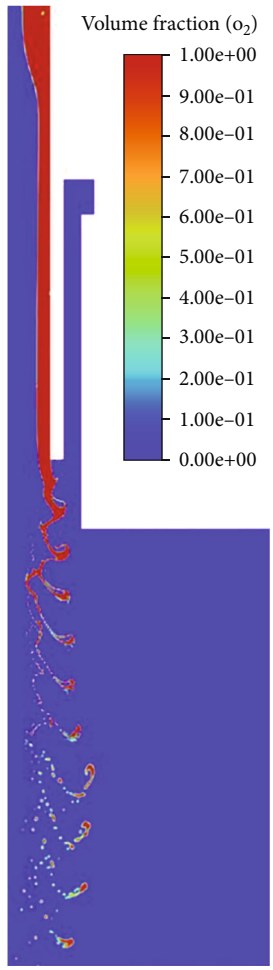

Figure 18: The contour of oxygen volume fraction when the flow rate of LOX $\dot{m}_l = 280$ g/s and the flow rate of GH_2 $\dot{m}_g = 161$ g/s (LOX/GH_2 mixing ratio = 1.74).

higher than the low-frequency pressure. Moreover, the dominant frequency of pressure oscillation is roughly distributed around 10000 Hz for these three conditions (Figures 13(a)–13(c)). In general, the dominant frequency of pressure oscillation increases from around 6000 Hz to around 10000 Hz as the flow rate of GH_2 that feeds to the injector decreases. And both high and low frequencies of pressure oscillation generally decrease with decreasing the flow rate of GH_2 (Figure 14). In addition, it can be seen from the pressure-time trace in Figure 13 that the reduction in the flow rate of GH_2 suppresses the amplitude range of pressure oscillations when the self-pulsation occurs.

3.2.2. The Effect of the Flow Rate of LOX. Five flow rates of LOX were selected according to the oxidizer-to-fuel mixing ratios corresponding to the operating conditions designed in the last subsection to investigate the effect of the flow rate of LOX on the self-pulsation characteristics. The specific operating parameters are shown in Table 4. The calculated contours of oxygen volume fraction for different flow rates of LOX when the self-pulsation occurs are shown in Figure 15.

According to the contours, it can be seen that when the flow rate of LOX is 101 g/s, the liquid film has already started to break into liquid droplets at the injector outlet. There is almost no continuous liquid filament downstream of the injector outlet. Compared with the following operating conditions, the liquid/gas ratio of 0.63 is relatively small at this time, so the process of liquid filament breaking into droplets transitions quickly. When the flow rate of LOX is 117 g/s, the liquid filament with good continuity starts to appear at the downstream position of the injector outlet. When the flow rate of LOX is 134 g/s, there are more liquid filaments and liquid lumps at the downstream. The continuity of liquid filament is better at the recess region, and the thickness of liquid film increases. At the flow rate of LOX of 149 g/s, the

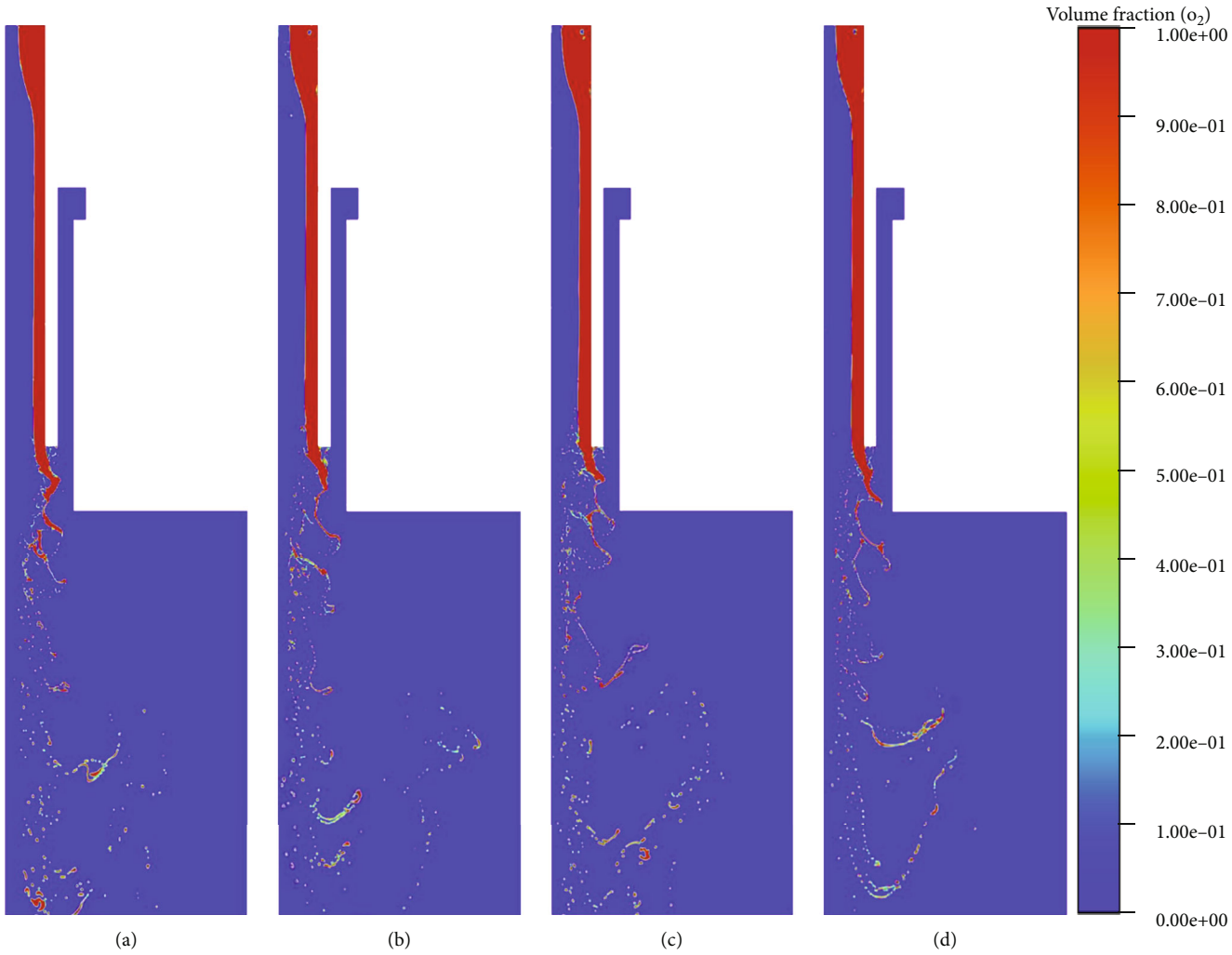

FIGURE 19: The contours of oxygen volume fraction under different initial temperature of GH_2: (a) $T = 33.7$ K; (b) $T = 43.7$ K; (c) $T = 53.7$ K; (d) $T = 63.7$ K.

numerous liquid lumps downstream of the outlet are connected to each other by a continuous liquid filament. And the number of large liquid filaments and large liquid lumps becomes more. The thickness of liquid film at the recess region also increased significantly. In addition, it can also be observed that at this time, due to the more intense degree of self-pulsation oscillation, the liquid filaments decomposed by the liquid film are distributed periodically and regularly in space. The performance is that strands of liquid lumps and filaments are continuously ejected from the injector outlet. When the flow rate of LOX increases to 165 g/s, the liquid film thickness at the recess region is larger. The continuity of the liquid filament at the outlet remains good. However, since the flow rate of GH_2 is relatively small compared to the LOX at this time, the self-pulsation performance is not so obvious. The liquid film breaks up irregularly into filaments and lumps from a position further downstream from the injector outlet. Obviously, the atomization performance at this time is poor. Overall, as the flow rate of LOX gradually increases, the thickness of the liquid film at the recess region becomes thicker. The continuity of the liquid filament becomes better and less likely to break. The degree of periodic self-pulsation oscillation becomes more and more severe at first and then turns into unstable random oscillation. The liquid filaments and lumps generated by the liquid film are also of different sizes and unevenly distributed in space.

The pressure-time plots and the frequency spectrum of pressure for different flow rate of LOX are presented in Figure 16. The high/low frequencies of pressure oscillations and their corresponding pressures (i.e., low-frequency pressure/high-frequency pressure) at different flow rates of LOX are extracted from these plots as depicted in Figure 17.

According to Figure 17, it can be seen that the low-frequency pressure decreases during the increase of the LOX flow rate from 101 g/s to 165 g/s. However, the high-frequency pressure increases first and then decreases. As in the case of changing the flow rate of GH_2, the dominant frequency of the self-pulsation oscillation changes during the increase of the flow rate of LOX. In the first two cases, the dominant frequency of pressure oscillation is still around 6000 Hz (Figures 16(a) and 16(b)). For the last three conditions, the dominant frequency of pressure oscillation is around 10000 Hz (Figures 16(c)–16(e)). This effect of the

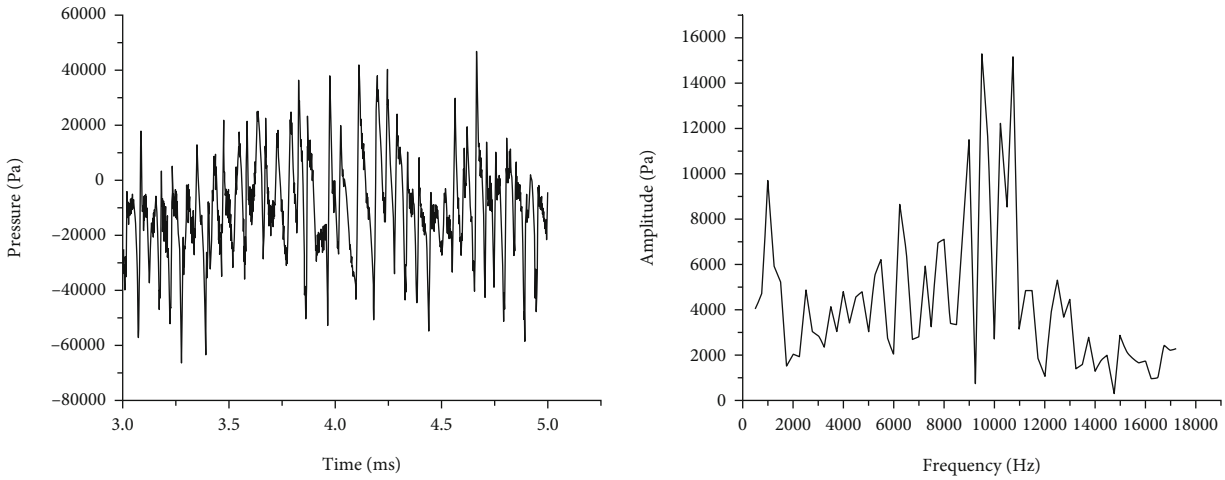

(a)

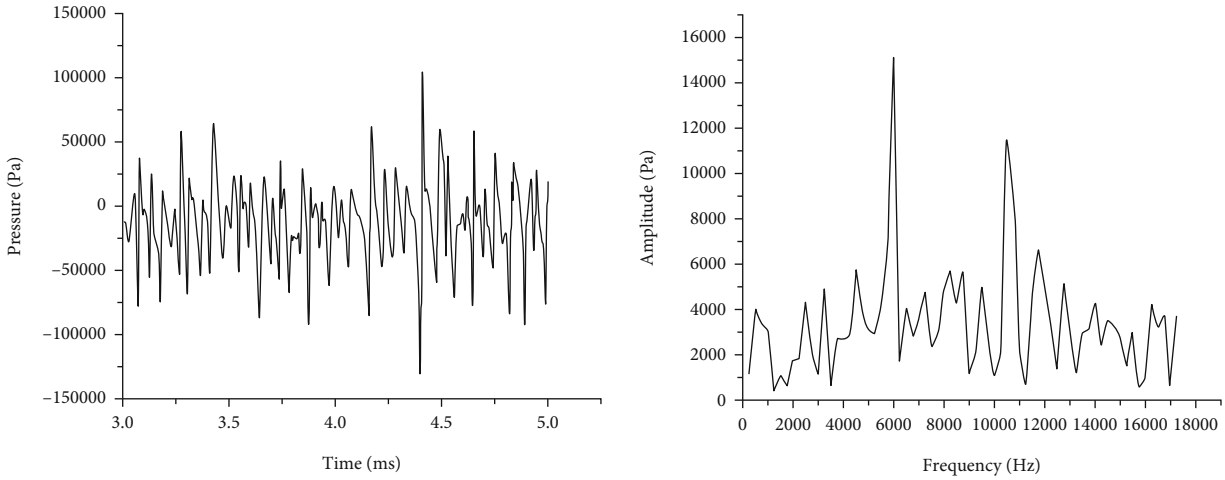

(b)

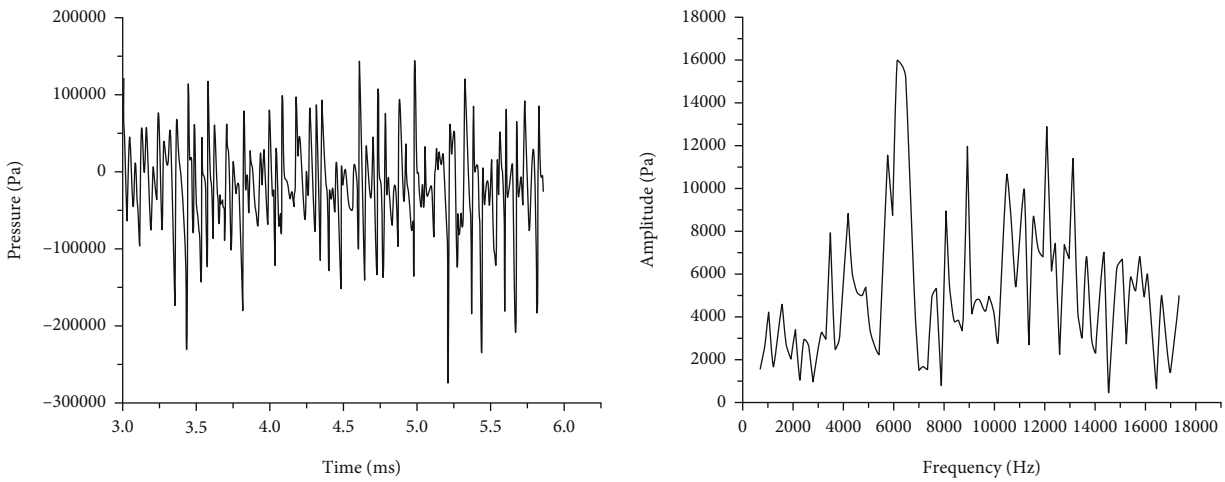

(c)

Figure 20: Continued.

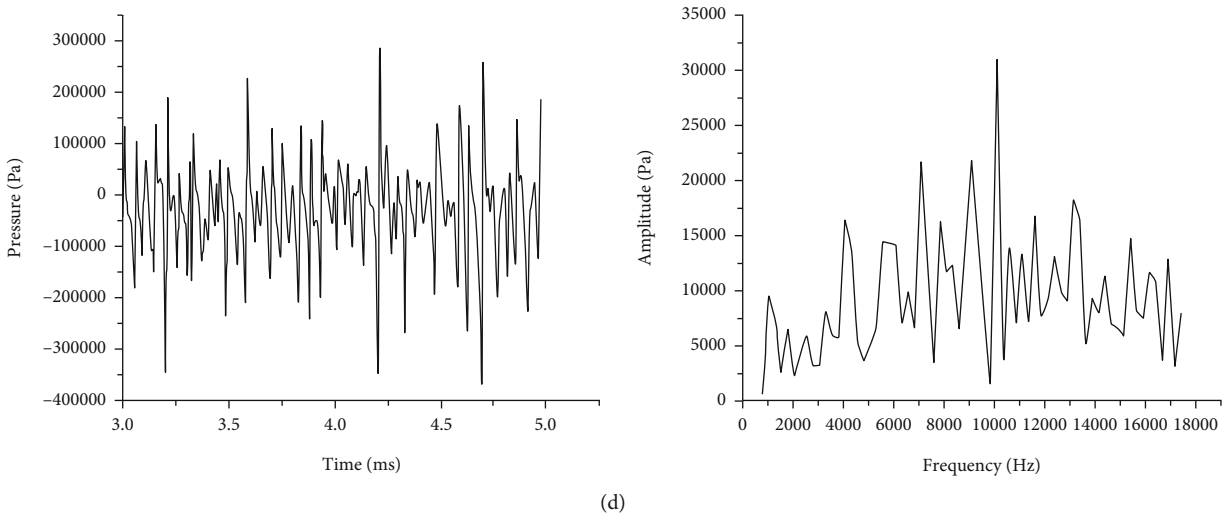

Figure 20: The pressure-time trace and frequency spectrum of pressure under different initial temperature of GH_2: (a) $T = 33.7$ K; (b) $T = 43.7$ K; (c) $T = 53.7$ K; (d) $T = 63.7$ K.

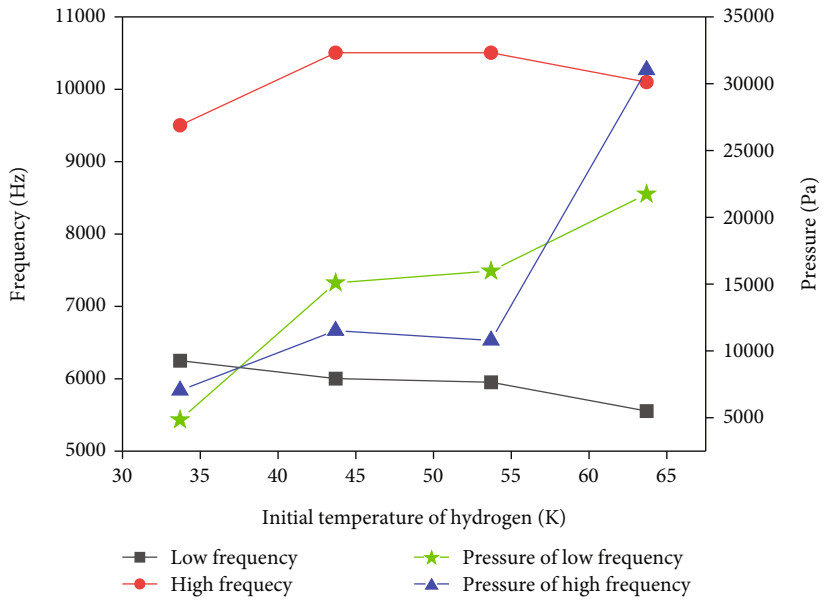

Figure 21: High/low frequencies of pressure oscillations under different initial temperature of GH_2 and their corresponding pressure.

LOX flow is similar to the effect brought by the GH_2 flow. That is, the self-pulsation oscillation at higher LOX/GH_2 mixing ratio has a larger dominant frequency of pressure oscillation; at lower LOX/GH_2 mixing ratios, the dominant frequency of pressure oscillation is also smaller. With the increase of the flow rate of LOX, the increase of high and low frequencies of pressure oscillation is not very significant (Figure 17). Moreover, it can be seen from the pressure-time curves in Figure 16 that the change of the flow rate of LOX does not have a great effect on the peak range of pressure oscillation during self-pulsation oscillation.

3.2.3. The Effect of the LOX/GH_2 Ratio. Combining the research results in sections 2.2.1 and 2.2.2, the effect of the LOX/GH_2 mixing ratio on the self-pulsation characteristics can be analyzed. Some phenomena and laws of the effect of the LOX/GH_2 mixing ratio on the spray morphology can be found. With the increase of mixing ratio, the liquid film thickness at the recess region gradually increases. The number of liquid filaments and liquid lumps gradually increases, and the continuity of liquid filaments becomes better. The position of the liquid filament massively broken into liquid droplets is increasingly moving downstream of the injector outlet. That is, the atomization performance of the injector will be deteriorated. In addition, the increase of the mixing ratio will intensify the phenomenon and degree of self-pulsation oscillation.

With the same mixing ratio, it is obvious that changing the flow rate of LOX has a greater effect on the liquid film thickness, the number of liquid filaments, and the position

of the broken into droplets than that when changing the flow rate of GH_2. To verify this conclusion, the flow rate of LOX was further increased to 280 g/s with reference to Table 4. The calculated contour plot of oxygen volume fraction is shown in Figure 18. It can be seen that the continuity of the liquid filament generated by the liquid film becomes significantly better at this working condition. The phenomenon of the self-pulsation oscillation is more significant. Liquid lumps and liquid filaments are sprayed from the injector in the form of periodic distribution in space. This spray pattern is macroscopically closer to the "Christmas tree" spray field in the experiment [20].

Combining the effects of flow rate of GH_2 and flow rate of LOX on the amplitude-frequency characteristics of the self-pulsation oscillation, it can be seen that either changing the flow rate of GH_2 or the flow rate of LOX, as long as the LOX/GH_2 mixing ratio increases, will make the dominant frequency of pressure oscillation change from low frequency to high frequency when self-pulsation occurs. However, the flow rate of GH_2 and the flow rate of LOX have different effects on the amplitude range of the pressure oscillation during self-pulsating. The effect of flow rate of GH_2 is greater than that of LOX. Therefore, the dominant frequency of pressure oscillation when self-pulsation occurs can be controlled from low to high frequency or from high to low frequency by adjusting the value of the LOX/GH_2 mixing ratio. This could prevent the pressure oscillation frequency of the self-pulsation of the injector from coupling with the acoustic oscillation frequency of the combustion chamber, thereby ensuring the safe operation of the engine.

3.2.4. The Effect of the Initial Temperature of GH_2. The initial temperature of the GH_2 supplied to the gas-liquid swirl coaxial injector would influence the unstable combustion in the engine. Considering that there is a certain correlation between self-pulsation oscillation and combustion instability, it is necessary to investigate the effect of the initial temperature of GH_2 on the self-pulsation characteristics. Four different operating conditions were arranged here, in which the flow rates of LOX and GH_2 were 134 g/s and 161 g/s, respectively. The initial temperatures of GH_2 for these conditions were 33.7 K, 43.7 K, 53.7 K, and 63.7 K. In this way, the effect of the initial temperature of GH_2 on the amplitude-frequency characteristics of the self-pulsation was investigated. The calculated contours of oxygen volume fraction at different initial temperatures of GH_2 are shown in Figure 19. The variations in the liquid film thickness at the recess region of the injector, as well as the change in the distribution of the liquid filaments and liquid lumps generated downstream, are not particularly obvious as the initial temperature of GH_2 increases. The phenomenon and extent of self-pulsation oscillations generated in the injector are not significantly enhanced by the increase of the initial GH_2 temperature. Therefore, the physical properties of propellants would not have an apparent impact on the flow and atomization characteristics of liquid sheet in the coaxial injector.

The pressure-time graphs and the frequency spectrum of pressure for different initial temperatures of GH_2 are shown in Figure 20. The high/low frequencies of pressure oscillations and their corresponding pressures for different initial temperatures of GH_2 were extracted from these graphs, as shown in Figure 21.

Figure 21 reveals that the variation of the initial temperature of GH_2 has little effect on the low/high frequencies of the pressure oscillation but has a great effect on the value of the oscillation pressure. Both the low-frequency pressure and the high-frequency pressure increase with the increase of the initial temperature of GH_2. In particular, the high-frequency pressure of self-pulsation is only 7045 Pa at the initial GH_2 temperature of 33.7 K. However, when the initial GH_2 temperature is 63.7 K, the high-frequency pressure of self-pulsation reaches 31029 Pa, which has a larger variation. The initial temperature of GH_2 also has a similar increasing effect on the low-frequency pressure of self-pulsation. In addition, referring to Figure 20, the change of the initial temperature would cause the dominant frequency of pressure oscillation to vary between the high and low frequencies.

4. Conclusions

Numerical investigations for the self-pulsation characteristics in supercritical state of a LOX/GH_2 swirl coaxial injector under various operating conditions have been presented. The GH_2 is axially injected into the recess chamber through the gas annulus, and the LOX is introduced from tangential holes. The RNG $k-\varepsilon$ turbulence model, VOF model, and PR state equations are employed to simulate the propellant injection process. The accuracy of the numerical model is verified by comparing with the experimental data. Specifically, the amplitude-frequency characteristics of the recess region, LOX, and GH_2 path when self-pulsation occurs are analyzed. The mechanism of the self-pulsation is also discussed. Besides, the effects of various operating parameters on the self-pulsation oscillation are clarified. The conclusions are drawn as follows.

(1) The self-pulsation mainly arises from the liquid sheet that periodically blocks the gas annulus at the recess region, which in turn causes periodic variations in the pressure and velocity at the injector outlet. The cyclic process of self-pulsation oscillation is dominated by two factors: the centrifugal force of the conical liquid sheet and the resistance of the surrounding annular gas flow to it

(2) When the self-pulsation occurs, the dominant frequencies of pressure oscillation in different regions (recess region, upstream of the LOX, or GH_2 path) are diverse. But for the monitoring points in each region, the dominant frequency is approximately the same. In the recess region, the closer to the downstream of the outlet and the position of the annular slit is, the lower the dominant pressure is. As moving downstream along the LOX path, the dominant pressure slightly decreases. As moving downstream along the GH_2 path, the dominant pressure first decreases slowly and then decreases significantly

(3) With increasing the LOX/GH_2 mixing ratio, the spray performance would be deteriorated observably.

The liquid film thickness at the recess region gradually increases. The position where the liquid filament is massively broken into droplets is further downstream of the outlet. With the same mixing ratio, changing the flow rate of LOX has a greater effect on the atomization features, such as liquid sheet thickness, filament continuity, and droplet size, than that when changing the flow rate of GH_2. The dominant frequency of pressure oscillation when self-pulsation occurs can be controlled to a high or low level by adjusting the LOX/GH_2 mixing ratio. This may prevent the pressure oscillation frequency coupling with the acoustic oscillation frequency in the combustion chamber

(4) The initial temperature of GH_2 rarely influences the flow and atomization characteristics (e.g., the liquid sheet thickness, the distribution of liquid filaments) while it would change the dominant frequency and corresponding pressure apparently during the self-pulsation. The pressures of low-frequency and high-frequency increase with the increase of the temperature. The variation of the initial temperature would shift the dominant frequency between the high and low regimes. Hence, more attentions should be paid to the fuel temperature to make sure the engine safety

Data Availability

The data used to support the findings of this study are available from the corresponding author upon request.

Conflicts of Interest

The authors declared no potential conflicts of interest with respect to the research, authorship, and/or publication of this article.

Acknowledgments

This work was supported by the National Natural Science Foundation of China (Grant Nos. 12272026, 11927802, and U1837211).

References

[1] G. P. Sutton, "History of liquid-propellant rocket engines in Russia, formerly the Soviet Union," *Journal of Propulsion and Power*, vol. 19, no. 6, pp. 1008–1037, 2003.

[2] D. K. Huzel, *Modern Engineering for Design of Liquid-Propellant Rocket Engines*, vol. 147, AIAA, 1992.

[3] Z. Kang, Z. G. Wang, Q. Li, and P. Cheng, "Review on pressure swirl injector in liquid rocket engine," *Acta Astronautica*, vol. 145, pp. 174–198, 2018.

[4] X. Bai, P. Cao, Q. Li, and P. Cheng, "The break phenomenon of self-pulsation for liquid-centered swirl coaxial injectors," *International Journal of Multiphase Flow*, vol. 142, article 103708, 2021.

[5] J. H. Im, D. Kim, Y. Yoon, T. Roh, and J. Koo, "Self-pulsation characteristics of a swirl coaxial injector with various injection and geometric conditions," in *41st AIAA/ASME/SAE/ASEE Joint Propulsion Conference & Exhibit, American Institute of Aeronautics and Astronautics*, p. 3749, Tucson, Arizona, 2005.

[6] V. Bazarov, "Self-pulsations in coaxial injectors with central swirl liquid stage," in *31st AIAA/ASME/SAE/ASEE Joint Propulsion Conference and Exhibit, American Institute of Aeronautics and Astronautics*, p. 2358, San Diego, California, 1995.

[7] D. T. Harrje, *Liquid Propellant Rocket Combustion Instability, Scientific and Technical Information Office*, vol. 194, National Aeronautics and Space Administration, 1972.

[8] V. Bazarov, "Influence of propellant injector stationary and dynamic parameters on high frequency combustion stability," in *32nd AIAA/ASME/SAE/ASEE Joint Propulsion Conference and Exhibit, American Institute of Aeronautics and Astronautics*, p. 3119, Lake Buena Vista, Florida, 1996.

[9] C. J. Eberhart and R. A. Frederick, "Parametric evaluation of swirl injector dynamics in the high-frequency range," *Journal of Propulsion and Power*, vol. 33, no. 5, pp. 1218–1229, 2017.

[10] C. J. Eberhart, D. M. Lineberry, and R. A. Frederick, "Detailing the stability boundary of self-pulsations for a swirl-coaxial injector element," in *Proc. of 49th AIAA/ASME/SAE/ASEE Joint Propulsion Conference and Exhibit*, San Jose, CA, California, 2013.

[11] C. J. Eberhart and R. A. Frederick, "Details on the mechanism of high-frequency swirl coaxial self-pulsation," *Journal of Propulsion and Power*, vol. 33, no. 6, pp. 1418–1427, 2017.

[12] Y. Huang, J. Zhou, X. Hu et al., "Acoustic model for the self-oscillation of coaxial swirl injector," in *33rd Joint Propulsion Conference and Exhibit, American Institute of Aeronautics and Astronautics*, p. 3328, Seattle, Washington, 1997.

[13] Y. Ren, W. Chu, Y. Tong, J. Zhao, W. Lin, and W. Nie, "Numerical investigation on spray self-pulsation characteristics of a liquid-centered swirl coaxial injector," *Aerospace Science and Technology*, vol. 112, article 106593, 2021.

[14] W. Chu, X. Li, Y. Tong, and Y. Ren, "Numerical investigation of the effects of gas-liquid ratio on the spray characteristics of liquid-centered swirl coaxial injectors," *Acta Astronautica*, vol. 175, pp. 204–215, 2020.

[15] S. Fechter, S. Karl, V. Hannemann, and K. Hannemann, "Simulation of LOx/GH2 single coaxial injector at high pressure conditions," in *53rd AIAA/SAE/ASEE Joint Propulsion Conference*, p. 4765, Atlanta Georgia, 2017.

[16] J. Tsohas and S. D. Heister, "Numerical simulations of liquid rocket coaxial injector hydrodynamics," *Journal of Propulsion and Power*, vol. 27, no. 4, pp. 793–810, 2011.

[17] X. Bai, L. Sheng, Q. Li, P. Cheng, and Z. Kang, "Effects of annulus width and post thickness on self-pulsation characteristics for liquid-centered swirl coaxial injectors," *International Journal of Multiphase Flow*, vol. 122, article 103140, 2020.

[18] X. Bai, P. Cheng, L. Sheng, Q. Li, X. Zhang, and Z. Kang, "Effects of backpressure on self-pulsation characteristics of liquid-centered swirl coaxial injectors," *International Journal of Multiphase Flow*, vol. 116, pp. 239–249, 2019.

[19] J. Ahn, H. Lim, G. Jeong, and K. Ahn, "Effect of the recess length on the dynamic characteristics of liquid-centered swirl coaxial injectors," *Acta Astronautica*, vol. 199, pp. 1–13, 2022.

[20] Z. Kang, Q. Li, P. Cheng, X. Zhang, and Z. Wang, "Effects of recess on the self-pulsation characteristics of liquid-centered swirl coaxial injectors," *Journal of Propulsion and Power*, vol. 32, no. 5, pp. 1124–1132, 2016.

[21] J. H. Im and Y. Yoon, "The effects of the ambient pressure on self-pulsation characteristics of a gas/liquid swirl coaxial injector," in *44th AIAA/ASME/SAE/ASEE Joint Propulsion Conference & Exhibit*, p. 4850, Hartford, Connecticut, 2008.

[22] C. J. Eberhart, *Investigation of Liquid Rocket Swirl Coaxial Injection Dynamics under Self-Excited High Frequency Oscillations*, Thesis, University of Alabama in Huntsville, USA, 2016.

[23] C. Hassa, J. Heinze, U. Meier, C. Heeger, P. Trunk, and A. Dreizler, "Self-exited oscillation in a combustion chamber driven by phase change in the liquid fuel feed system," *International Journal of Spray and Combustion Dynamics*, vol. 3, no. 4, pp. 273–284, 2011.

[24] X. Qiao, *Study on the Characteristics of Self-Pulsation of Gas-Liquid Swirl Coaxial Injector under Supercritical Condition*, Thesis, China Academy of Launch Vehicle Technology, Beijing, China, 2022.

[25] M. Tajnesaie, N. E. Jafari, R. Barati, and M. M. Azhdary, "Performance comparison of four turbulence models for modeling of secondary flow cells in simple trapezoidal channels," *ISH Journal of Hydraulic Engineering*, vol. 26, no. 2, pp. 187–197, 2020.

[26] Y. Ren, K. Guo, J. Zhao, W. Nie, Y. Tong, and W. Chu, "Numerical investigation of spray self-pulsation characteristics of liquid-centered swirl coaxial injector with different recess lengths," *International Journal of Multiphase Flow*, vol. 138, article 103592, 2021.

[27] V. Yakhot and S. A. Orszag, "Renormalization group analysis of turbulence. I. Basic theory," *Journal of Scientific Computing*, vol. 1, no. 1, pp. 3–51, 1986.

[28] B. L. Wang, P. C. Miles, R. D. Reitz, Z. Han, and B. Petersen, "Assessment of RNG turbulence modeling and the development of a generalized RNG closure model," SAE Technical Paper No. 2011-01-0829, 2011.

[29] M. Sussman and E. G. Puckett, "A coupled level set and volume-of-fluid method for computing 3D and axisymmetric incompressible two-phase flows," *Journal of Computational Physics*, vol. 162, no. 2, pp. 301–337, 2000.

[30] C. W. Hirt and B. D. Nichols, "Volume of fluid (VOF) method for the dynamics of free boundaries," *Journal of Computational Physics*, vol. 39, no. 1, pp. 201–225, 1981.

[31] G. A. Melhem, R. Saini, and B. M. Goodwin, "A modified Peng-Robinson equation of state," *Fluid Phase Equilibria*, vol. 47, no. 2-3, pp. 189–237, 1989.

[32] R. I. Issa, "Solution of the implicitly discretised fluid flow equations by operator-splitting," *Journal of Computational Physics*, vol. 62, no. 1, pp. 40–65, 1986.

[33] X. Bai, Q. Li, P. Cheng, L. Sheng, and Z. Kang, "Investigation of self-pulsation characteristics for a liquid-centered swirl coaxial injector with recess," *Acta Astronautica*, vol. 151, pp. 511–521, 2018.